Geochemistry and Crystallization Conditions of Magmas Related to Porphyry Mo Mineralization in Northeastern China

Hegen Ouyang,[1,2] Jingwen Mao,[2,†] and Ruizhong Hu[1,3]

[1]*State Key Laboratory of Ore Deposit Geochemistry, Institute of Geochemistry, Chinese Academy of Sciences, Guiyang, 550081, China*

[2]*MNR Key Laboratory of Metallogeny and Mineral Assessment, Institute of Mineral Resources, Chinese Academy of Geological Sciences, Beijing, 100037, China*

[3]*College of Earth and Planetary Sciences, University of Chinese Academy of Sciences, Beijing, 100049, China*

Abstract

To better understand processes leading to porphyry Mo deposit formation, the metal content, volatile content, and crystallization conditions of melt inclusions from pre- and synmineralization intrusions in six porphyry(-skarn) Mo deposits of northeastern China (Aolunhua, Hashitu, Lanjiagou, Songbei, Wanbaoyuan, and Yangjiazhangzi) were investigated by means of laser ablation-inductively coupled plasma-mass spectrometry and electron microprobe analysis. The ore-forming silicate melts were one to four times more evolved than average granite with 1 to 7 ppm Mo. The ore-related intrusions crystallized predominantly at 760° to 690°C and 3.7 to 1.0 kbar, except for the one at Hashitu, which crystallized at 770° to 740°C and lower pressures (2.0–1.0 kbar). Fertile silicate melts at Hashitu contain up to 0.4 wt % F, 0.03 to 0.09 wt % Cl, 5.0 to 7.0 wt % H_2O, 10 to 24 ppm Cs, and 200 to 500 ppm Rb, whereas those at Yangjiazhangzi and Wanbaoyuan contain less Cs (3–6 ppm and 5–7 ppm, respectively), less Rb (180–220 ppm and 200–240 ppm, respectively), and negligible F (<0.15 wt %) but have similar Cl (0.03–0.05 wt %) and H_2O (5.3–6.5 wt % and 4.0–5.2 wt %, respectively) contents. Calculated melt viscosities in fertile magmas (log η = 4.3–6.1 Pa s) are at the lower end of the values reported for felsic melts at the same temperature.

Comparison between syn- and premineralization intrusions in individual deposits reveals that the ore-related intrusions were similarly evolved and had similar Mo contents and crystallization conditions as the nonmineralizing intrusions. The only difference is that the premineralization intrusions tend to occur as batholiths. The key to porphyry Mo mineralization lies in the focusing of fluid into and through a small rock volume on the top of the intrusion.

For the studied porphyry Mo deposits, the mineralizing magmas are all Mo poor, indicating Mo enrichment is not required to form porphyry Mo deposits. Metal endowments in porphyry Mo deposits have no direct relationship with the composition and crystallization condition of mineralizing melts but are linked with the fluid flux released from the underlying magma chamber through a cupola.

Introduction

Porphyry Mo deposits (defined as containing >0.05 wt % Mo and an Mo/Cu ratio >1; Carten et al., 1993), together with porphyry Cu-Mo deposits, are our most important sources of Mo. These deposits are characterized by a stockwork of molybdenite ± quartz ± pyrite ± K-feldspar ± biotite ± fluorite veins that are spatially and genetically related to felsic, porphyritic, plug-shaped intrusions. Porphyry Mo deposits were traditionally grouped into two classes based on the characteristics displayed by the deposits in western North America (White et al., 1981; Carten et al., 1993; Ludington and Plumlee, 2009; Taylor et al., 2012): (1) Climax-type porphyry Mo deposits, which are associated with F-rich (commonly >1.0 wt %), highly evolved rhyolitic magmas (e.g., Climax, Henderson-Urad, and Questa) generated in a within-plate tectonic environment, and (2) Endako-type porphyry Mo deposits, which are associated with low-F (usually less than 0.1 wt %), differentiated calc-alkaline granitoids in arc settings (e.g., Endako, Quartz Hill, and Logtung). Climax-type porphyry Mo deposits have generally received more attention than arc-related porphyry Mo deposits because of their higher ore grade (typically 0.1–0.3 wt % Mo; Ludington and Plumlee, 2009) and the peculiar geochemical characteristics of the associated magmas (e.g., enriched in F, Rb, Nb, and Ta; Ludington and Plumlee, 2009).

In the past 10 to 20 years, China has emerged as the country with the largest Mo reserves (8,300 Mt). It is now the world's largest Mo producer (2017 production ≈ 130,000 t Mo metal; U.S. Geological Survey, 2017). However, many Chinese porphyry Mo deposits proved to be difficult to classify with the tectonic classification schemes proposed by Carten et al. (1993), Ludington and Plumlee (2009), and Taylor et al. (2012), because many of them formed in response to continental collision rather than due to subduction or incipient rifting, in contrast to the deposits of the Rocky Mountains of western North America (Carten et al., 1993; Ludington and Plumlee, 2009). For this reason, a new class of deposits, called postcollisional- or Dabie-type porphyry Mo deposits, has been proposed, in particular for the occurrences within the Dabie-Qinling orogenic belt (e.g., Chen et al., 2017). Although much has been learned in the past few decades about the nature of ore-forming melts in Climax-type porphyry Mo deposits through the analysis of fluid and melt inclusions (e.g., Lowenstern, 1995; Audétat, 2010, 2015; Zhang and Audétat, 2017), relatively little is known about the nature of melt inclusions from Chinese porphyry Mo deposits. Lowenstern (1994) and Shinohara et al. (1995) proposed a magma convection model for Climax-type deposits to explain how Mo can be extracted

†Corresponding author: e-mail, jingwenmao@263.net

efficiently from voluminous Mo-poor magma (2–25 ppm Mo; Audétat and Li, 2017, and references therein). In their model, copious amounts of bubbly magmas (i.e., Mo-laden, fluid-rich magmas) were delivered through the magma chamber into the cupola by means of weight-derived magma convection. However, it is not clear whether this model is also applicable to Endako- and Dabie-type porphyry Mo deposits, as the geochemistry and crystallization conditions of magmas related to these two types of deposits have not been well constrained.

In this study, we investigated samples from six large (0.12–1.7 Mt Mo) porphyry(-skarn) Mo deposits in northeastern China that range in age from Early Jurassic to Early Cretaceous and vary in terms of tectonic setting from within a reactivated craton margin (Yangjiazhangzi, Songbei, and Wanbaoyuan) to within a composite accretionary orogen (Aolunhua and Hashitu; Fig. 1). The main focus of this study is on melt inclusions, small droplets of silicate melt that were trapped during the growth of magmatic phenocrysts and are able to provide information on the original metal and volatile content of the melt at various degrees of magma evolution (e.g., Lowenstern, 1995; Frezzotti, 2001; Webster, 2006;

Audétat et al., 2008; Audétat and Lowenstern, 2014). The aim of this study is to (1) provide a detailed assessment of the composition of melts in the magmas associated with porphyry (-skarn) Mo deposits in northeast China, (2) compare the melt inclusion data with similar data obtained from Climax-type porphyry Mo deposits, and (3) discuss the results in light of the genetic model proposed for the genesis of porphyry Mo deposits.

Geologic Background

A regional-scale geologic and tectonic map of northeastern China showing the location of the six investigated porphyry Mo deposits is shown in Figure 1. Four of them (Yangjiazhangzi, Songbei, Lanjiagou, and Wanbaoyuan) are located within the North China craton; the other two (Aolunhua and Hashitu) are located within the Central Asian orogenic belt. Yangjiazhangzi, Songbei, and Lanjiagou formed between 191 and 183 Ma, and the others formed between 147 and 130 Ma. The Early Jurassic deposits may have formed in an active continental margin related to the northwestward subduction of the Paleo-Pacific plate (e.g., Davis et al., 2001; Chen et al., 2007).
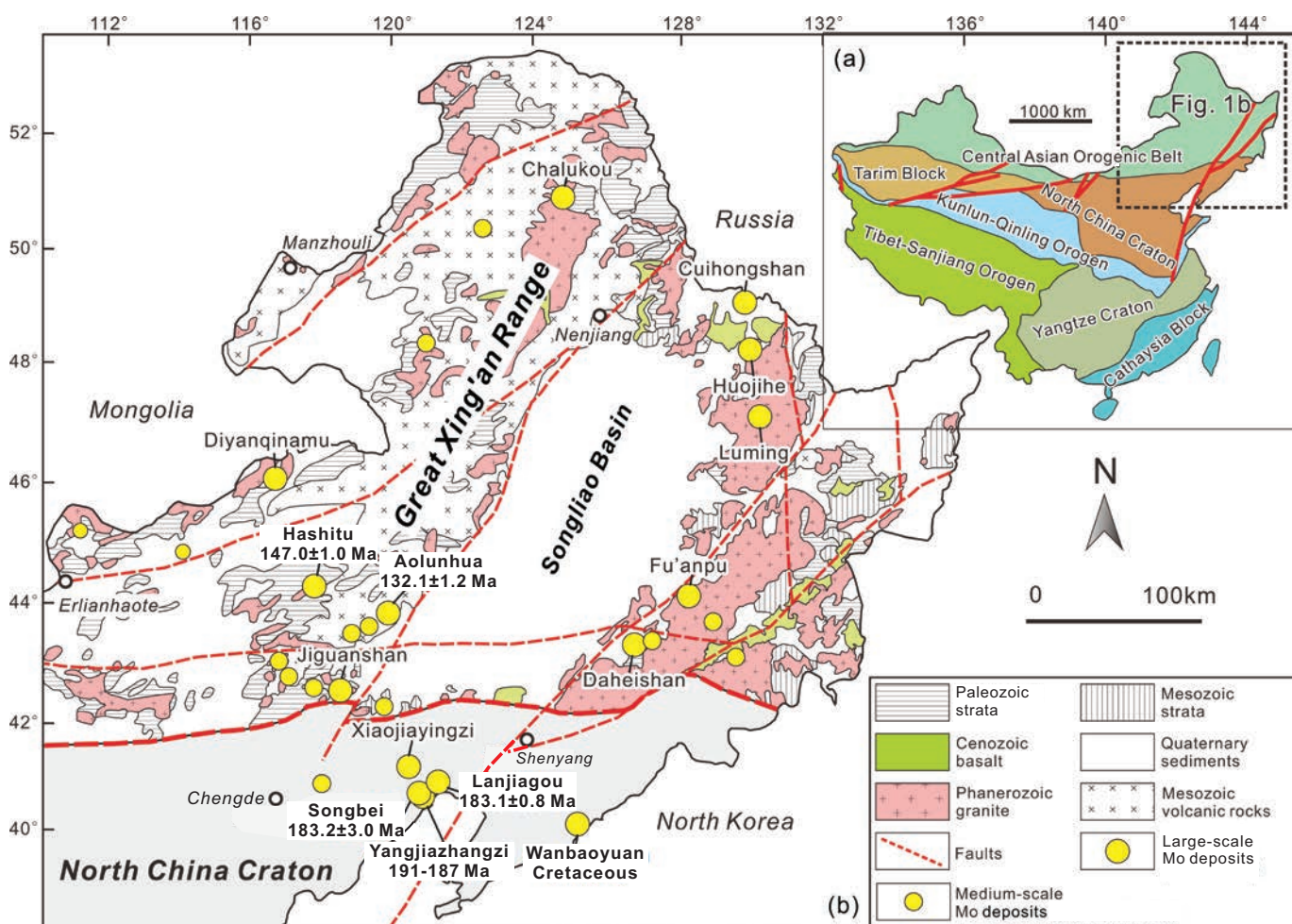

Fig. 1. (a) Simplified geologic map of China, showing the main tectonic units. (b) Simplified geologic map of northeastern China and surrounding regions, showing major geologic units, geographical reference points, and the locations of major porphyry(-skarn) Mo deposits (modified from Ouyang et al., 2013). Mineralization ages taken from Yang et al. (1989), Huang et al. (1994), Ma et al. (2009), Han et al. (2009), Zhai et al. (2014), and Chu et al. (2017).

Alternatively, a postcollisional extensional setting related to collision between the North China craton and the amalgamated terranes of Central Asian orogenic belt (Xiao et al., 2003) has been proposed based on the contemporary development of rift basins, alkaline complexes, mafic-ultramafic complexes, and bimodal volcanism in the eastern part of the North China craton (Yang et al., 2006; Guo et al., 2007; Zhang et al., 2014). Early Cretaceous mineralization was contemporary with the exhumation of metamorphic core complexes, extensive mafic to felsic magmatism, and the development of intracontinental rift basins throughout northeastern China—events that have been interpreted to indicate crustal extension and asthenospheric upwelling (Wu et al., 2011, and references therein; Xu et al., 2013). These processes may relate to orogenic collapse after the collision between the Central Asian orogenic belt and Siberia craton (Meng, 2003), rollback of the subducted Paleo-Pacific plate during the Late Jurassic (Wang et al., 2006; Li et al., 2012; Zhang et al., 2014), or a combination of both phenomena (Wu et al., 2011).

Yangjiazhangzi Mo deposit

Yangjiazhangzi is located in the eastern part of the North China craton (Fig. 1b), an Archean craton that has undergone lithospheric thinning since the early Mesozoic (Gao et al., 2004; Xu et al., 2006). The deposit contains 0.26 Mt Mo at an average grade of 0.14% (Huang et al., 1989). Molybdenum mineralization occurs mainly in Precambrian carbonate rocks at the southern margin of the large Yangjiazhangzi pluton (Wu et al., 1990; Fig. 2a). The Yangjiazhangzi pluton contains coarse-grained syenogranite with minor fine-grained syenogranite and granite porphyry (Huang et al., 1994; Wu et al., 2006). The coarse-grained syenogranite varies from equigranular to porphyritic and was intruded by the fine-grained syenogranite and granite porphyry (Fig. 2a; Huang et al., 1994). A general lack of quartz veins coupled with only weak sericite alteration of the coarse-grained syenogranite (Fig. 3a) that occurred away from the skarn mineralization center for about 100 m (App. Fig. S1) suggests that the coarse-grained syenogranite was emplaced before mineralization. The fine-grained
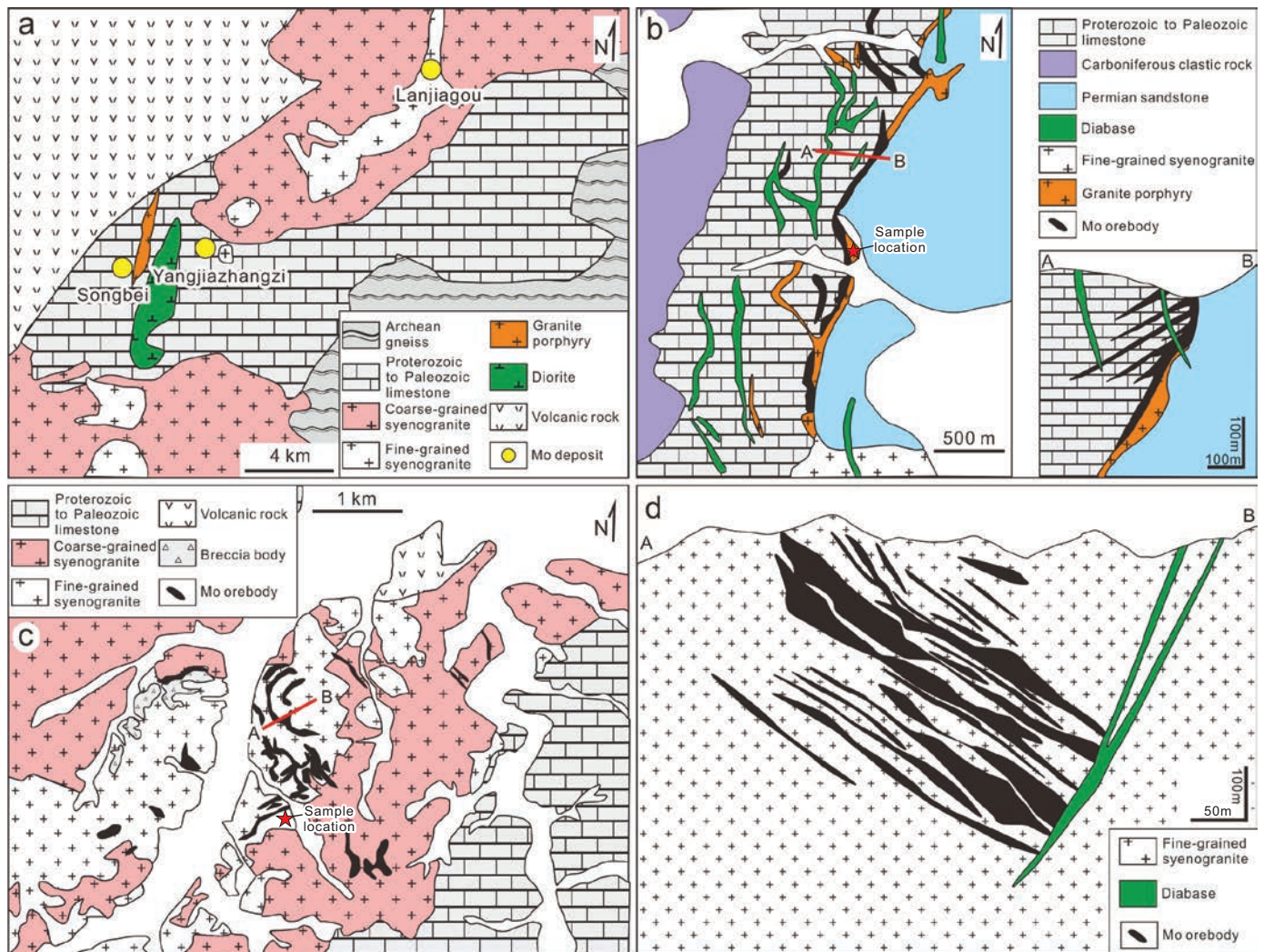

Fig. 2. (a) Simplified geologic map of the area around the Yangjiazhangzi, Lanjiagou, and Songbei deposits (modified from Wu et al., 1990). (b) Geologic map and cross section of Songbei (Chu et al., 2017). (c) Geologic map of Lanjiagou (Han et al., 2009). (d) Geologic cross section through Lanjiagou (see Fig. 2c for the location of the section; Zheng et al., 2014).
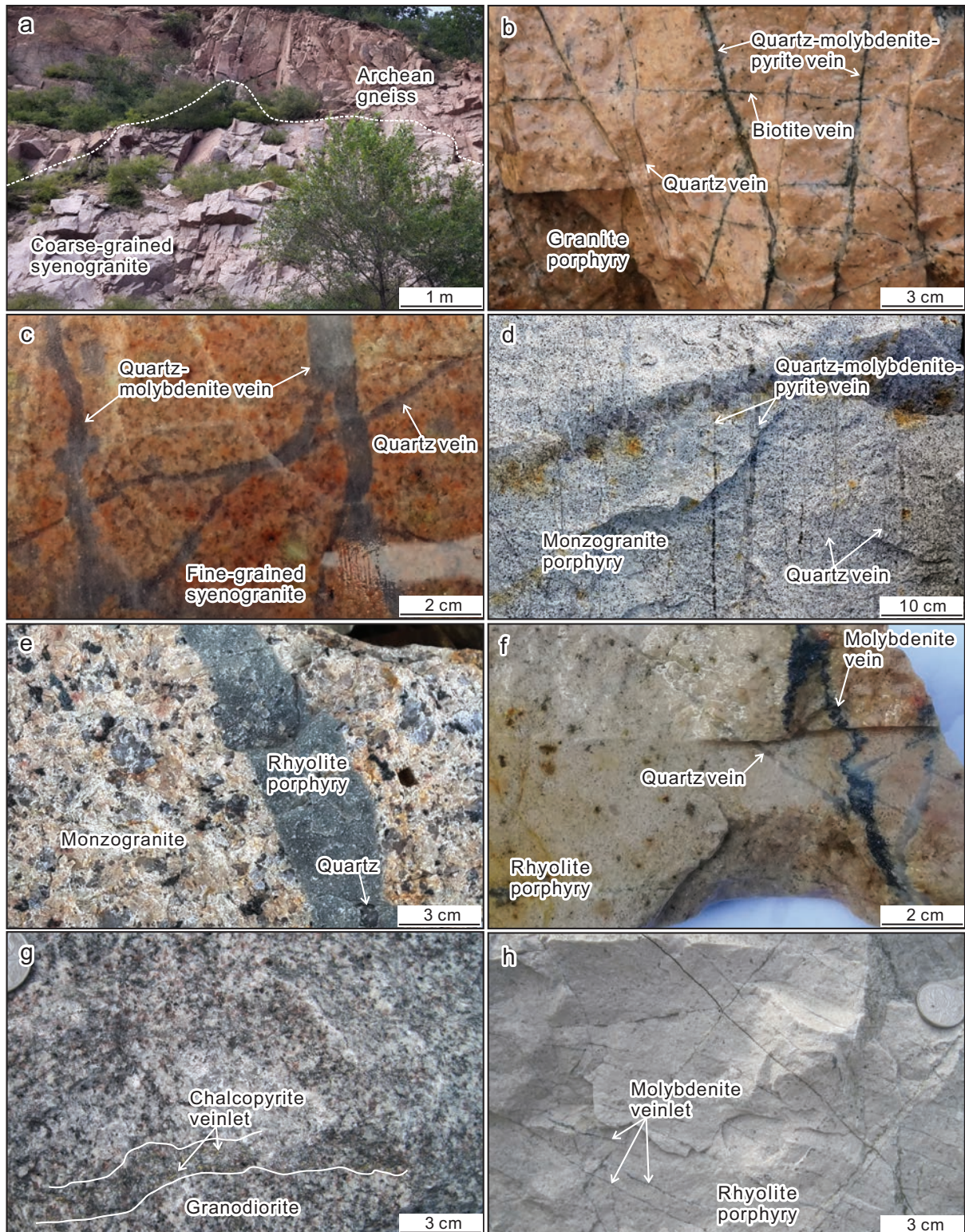
Fig. 3. Representative photographs showing the geologic relationships of intrusions and veins described in this study. (a) Yangjiazhangzi coarse-grained syenogranite intruding into Archean gneiss. (b) Songbei granite porphyry cut by biotite vein, in turn cut by quartz veins with K-feldspar halos and quartz-molybdenite-pyrite veins with sericite alteration envelopes. (c) Lanjiagou fine-grained syenogranite cut by quartz vein with K-feldspar envelopes, in turn truncated by quartz-molybdenite veins. (d) Aolunhua monzogranite porphyry cut by quartz with fine-grained K-feldspar halos and quartz-molybdenite veins. (e) Hashitu monzogranite truncated by rhyolite porphyry. (f) Hashitu rhyolite porphyry cut by quartz with K-feldspar halos and quartz-molybdenite veins. (g) Wanbaoyuan granodiorite truncated by chalcopyrite veinlets with sericite and chlorite alteration halos. (h) Wanbaoyuan rhyolite porphyry with molybdenite veinlets.

syenogranite and granite porphyry intruded Precambrian carbonate rocks and produced skarn mineralization. Therefore, these two phases are interpreted as synmineralization intrusions. Whole-rock analyses of the synmineralization phases of the Yangjiazhangzi pluton are similar with respect to their major elements (SiO_2 = 71–77 wt %, K_2O = 4.1–5.5 wt %; A/CNK = molar Al_2O_3/(CaO + Na_2O + K_2O), 0.9–1.1), trace elements (La_N/Yb_N = 7.7–9.1, δEu = 0.6–0.7), and O isotope composition ($\delta^{18}O‰$ = 8.1–8.8; Wu et al., 1990; App. Table S1). Zircon U-Pb dating of the fine-grained syenogranite gives ages ranging from 189.0 ± 4.0 to 188.0 ± 2.0 Ma (Wu et al., 2006), contemporaneous with molybdenite Re-Os mineralization ages of 191.0 ± 6.0 to 187.0 ± 2.0 Ma (Huang et al., 1994). The Songshuluo diorite crops out about 1.0 km west of the mine (Fig. 2a). It has a zircon U-Pb age of 221.0 ± 2.0 Ma (Wu et al., 2006), indicating that it is a premineralization intrusion. Melt inclusion analysis samples were obtained from the granite porphyry phase of the premineralization syenogranite (Yang 4, Fig. 4a), and from the granite porphyry phase (Yang 5, Fig. 4b) and rhyolite porphyry phase (Yang 1 and Yang 2, Fig. 4c) from the synmineralization intrusion (Table 1).

Songbei Mo deposit

Songbei is located ~3.0 km west of Yangjiazhangzi (Fig. 2a). It has an indicated resource of 0.17 Mt Mo at an average grade of 0.10% (Zeng et al., 2013). Intrusive rocks throughout the mining area comprise fine-grained syenogranite, granite porphyry, and diabase (Fig. 2b). The fine-grained syenogranite stock crops out to the south of the deposit and was intruded by pink granite porphyry. The main body of granite porphyry intruded along the contact between Permian sandstone and Proterozoic to Paleozoic limestone, and into the limestone itself, where most of the Mo mineralization occurs. Biotite and quartz veins with K-feldspar alteration halos affected this intrusion (Fig. 3b), indicating the granite porphyry was a synmineralization body. Zircon U-Pb dating of granite porphyry yielded an Early Jurassic age (184.0 ± 2.0 Ma), contemporaneous with Mo mineralization (molybdenite Re-Os age of 183.2 ± 3.0 Ma; Chu et al., 2017). The granite porphyries are silica (74–76 wt %) and K_2O rich (4.7–5.6 wt %) and metaluminous to mildly peraluminous with A/CNK between 1.0 and 1.1 (Chu et al., 2017). They are characterized by moderate fractionation between light rare earth elements (LREEs) and heavy rare earth elements (HREEs) (La_N/Yb_N = 2.6–15.2), strongly negative Eu anomalies (δEu = 0.1–0.5), and enriched Hf isotope compositions ($\varepsilon_{Hf}(t)$ values from –10.0 to –6.9), indicating that their parental magmas were produced by partial melting of ancient lower crust of the North China craton (Chu et al., 2017). Unaltered diabase dikes crosscut the Mo orebodies (Fig. 2b). Two samples of rhyolite porphyry phase from the synmineralization intrusion (Song 1 and Song 2, Fig. 4g), which proved suitable for melt inclusion analyses, were identified in the Songbei open pit.

Lanjiagou Mo deposit

Lanjiagou is located ~20 km northwest of Yangjiazhangzi (Fig. 2a). It has an indicated resource of 0.22 Mt Mo at an average grade of 0.13% (Huang et al., 1989). Lanjiagou has been divided into the upper Lanjiagou, middle Lanjiagou, lower Lanjiagou, Xiaomagou, Yuanbaoshan, and Xishan ore blocks.

In all blocks, mineralization is characterized by molybdenite-bearing quartz veins hosted by the Lanjiagou pluton. The Lanjiagou pluton crops out continuously over an area of ~20 km² and consists of coarse-grained syenogranite and fine-grained syenogranite (Fig. 2c, d). The coarse-grained syenogranite constitutes the bulk of the pluton and was intruded by synmineralization fine-grained syenogranite that contains A-type veins (Figs. 3c, 4h). Whole-rock analyses of the fine-grained syenogranite show that it is silica (75–76 wt %) and K_2O rich (4.5–6.6 wt %) and metaluminous to mildly peraluminous (A/CNK = 0.96–1.06), with strong fractionation between LREEs and HREEs (La_N/Yb_N = 9.4–31.3) and moderate negative Eu anomalies (δEu = 0.5–0.7; Dai et al., 2008; this study). The fine-grained syenogranite has a U-Pb zircon age of 185.0 ± 1.8 Ma (Zheng et al., 2014), which agrees within error with the Re-Os age of 183.1 ± 0.8 Ma for molybdenite (Han et al., 2009). As is the case at Songbei, the coarse- and fine-grained syenogranite and the orebodies are cut by NE-trending unaltered diabase dikes (Fig. 2d). Only one sample of the synmineralization phase (Lanji 7, Fig. 4h) was included in the melt inclusion study, owing to the poor preservation state of the melt inclusions.

Aolunhua Mo deposit

Aolunhua is situated in the Great Xing'an Range, which is a part of the eastern segment of the Central Asian orogenic belt (Xiao et al., 2003; Fig. 1). It was formed in a postsubduction setting related to the rollback of the Paleo-Pacific plate in the east and the closure of Mongolia-Okhotsk Ocean in the northwest (Meng, 2003; Wu et al., 2005; Xu et al., 2013). The deposit contains an inferred resource of 1.70 Mt Mo at an average grade of 0.05% (Chen et al., 2012). Mineralization is characterized by molybdenite-bearing quartz veins (0.5–3.0 cm wide) in the monzogranite porphyry (Fig. 3d; App. Fig. S1c), which is the main intrusion at Aolunhua (Fig. 5a). In the center of the intrusion, the monzogranite porphyry grades into an equigranular monzogranite. Both the monzogranite porphyry and the equigranular monzogranite contain abundant mafic microgranular enclaves (MMEs) of dioritic to quartz monzodioritic composition (Ma et al., 2013). Zircon U-Pb dating of the monzogranite porphyry and MMEs returned ages of 131.9 ± 0.5 and 132.2 ± 1.1 Ma (Ma et al., 2013), respectively, which are in agreement with the Re-Os age of 132.1 ± 1.2 Ma obtained from molybdenite (Ma et al., 2009). The monzogranite porphyry is crosscut by barren quartz porphyry and diorite dikes (Fig. 5a). Zircon U-Pb dating of the dikes indicates they intruded at 125.7 ± 0.6 Ma (Ma et al., 2013)—i.e., their emplacement postdates the ore-forming hydrothermal event by about 6 m.y. The monzogranite porphyry has SiO_2 contents of 68 to 70 wt % and K_2O contents of 3.4 to 4.5 wt %, and is metaluminous (A/CNK = 0.9–1.0) in composition (Ma et al., 2013). It is characterized by a high fractionation between LREEs and HREEs (La_N/Yb_N = 12.7–23.6), a negligible Eu anomaly (δEu = 0.9–1.0), and a high Sr/Y ratio (55–80; Ma et al., 2013). Its Sr-Nd-Hf isotope signatures ($^{87}Sr/^{86}Sr_i$ = 0.7049–0.7052, $\varepsilon_{Nd}(t)$ = 0.5–1.4, $\varepsilon_{Hf}(t)$ = 3.5–9.8) and the occurrence of MMEs indicate that it was derived by mixing of juvenile crust-derived felsic magma with previously metasomatized lithospheric mantle-derived mafic magma (Ma et al., 2013). Only one sample of
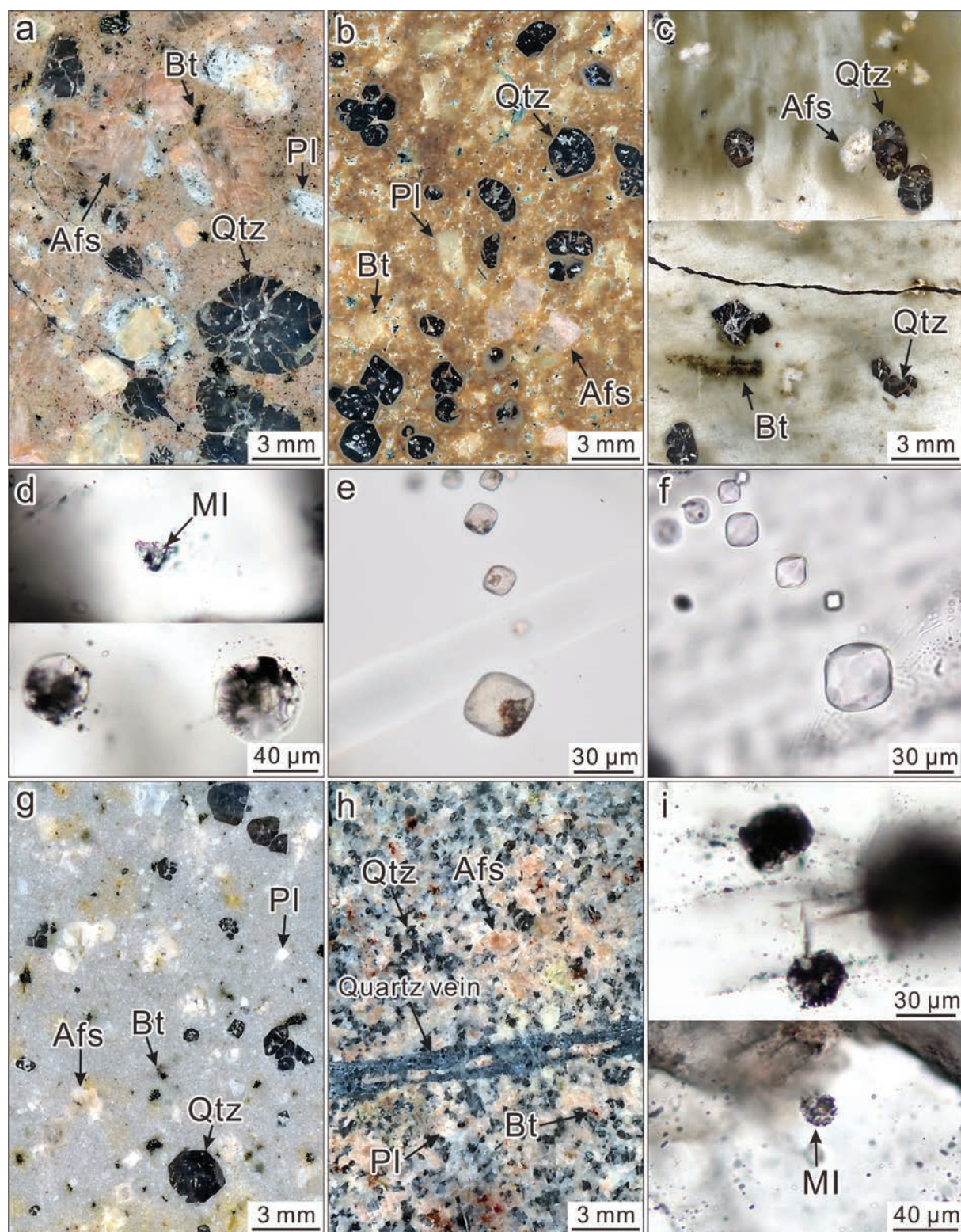
Fig. 4. Photographs of polished thick sections and melt inclusions in quartz phenocrysts and matrix quartz. (a) Yangjiazhangzi granite porphyry sample Yang 4. (b) Yangjiazhangzi granite porphyry sample Yang 5. (c) Yangjiazhangzi rhyolite porphyry sample Yang 2. (d) Coarsely crystallized melt inclusion in sample Yang 4 (top) and finely crystallized melt inclusions in sample Yang 5 (bottom). (e) Finely crystallized melt inclusions in sample Yang 2. (f) The same melt inclusions as shown in (e), after homogenization at 2.0 kbar and 780°C in a rapid-quench cold-seal pressure vessel. (g) Songbei rhyolite porphyry sample Song 1. (h) Lanjiagou fine-grained syenogranite sample Lanji 7 cut by quartz vein with fine-grained K-feldspar halos. (i) Decrepitated, finely crystallized melt inclusions in sample Song 1 (top) and finely crystallized melt inclusion in sample Lanji 7 (bottom). Abbreviations: Afs = alkali feldspar, Bt = biotite, MI = melt inclusion, Pl = plagioclase, Qtz = quartz.

Table 1. Summary of the Age and Petrography in Samples Investigated from the Porphyry(-Skarn) Mo Deposits in this Study

Deposit	Intrusion phase	Age (Ma)	Timing	Sample no.	Sample location	Phenocrysts	Magmatic accessory phases
Aolunhua[1]	Monzogranite porphyry	131.2 ± 1.9	Synmineralization	Aolu 11	120°13'31" E, 44°32'25" N 638 m	Quartz, alkali feldspar, plagioclase, biotite	Apatite, titanite, zircon, Fe-Ti oxides
Hashitu[2]	Monzogranite	147.0 ± 1.0	Premineralization	Hash 13	118°01'03" E, 44°04'24" N 1,292 m	Quartz, alkali feldspar, plagioclase, biotite	Zircon, Fe-Ti oxides
Hashitu[2]	Porphyritic monzogranite	147.0 ± 1.0	Premineralization	Hash 10	118°01'03" E, 44°04'24" N 1,292 m	Quartz, alkali feldspar, plagioclase, biotite	Zircon, Fe-Ti oxides
Hashitu	Granite porphyry	No data	Synmineralization	Hash 5	120°01'02" E, 44°04'23" N 1,283 m	Quartz, alkali feldspar, plagioclase, biotite	Zircon, Fe-Ti oxides
Hashitu	Rhyolite porphyry	No data	Synmineralization	Hash 6, Hash 7	120°01'02" E, 44°04'23" N 1,283 m	Quartz, alkali feldspar, plagioclase, biotite	Zircon, Fe-Ti oxides, molybdenite
Lanjiagou[3]	Fine-grained syenogranite	185.0 ± 1.8	Synmineralization	Lanji 7	120°37'56" E, 40°52'53" N 219 m	Quartz, alkali feldspar, plagioclase, biotite	Zircon, Fe-Ti oxides, apatite, titanite
Songbei[4]	Rhyolite porphyry	184.0 ± 2.0	Synmineralization	Song 1, Song 2	120°27'02" E, 40°47'57" N 186 m	Quartz, alkali feldspar, plagioclase, biotite	Apatite, titanite, zircon, Fe-Ti oxides
Wanbaoyuan[5]	Granodiorite	Ca. 130	Premineralization	Wan 10	125°28'24" E, 40°44'52" N 127 m	Quartz, plagioclase, alkali-feldspar, biotite, hornblende	Zircon, titanite, apatite, Fe-Ti oxides
Wanbaoyuan[5]	Rhyolite porphyry	No data	Synmineralization	Wan 1, Wan 2, Wan 3	125°28'24" E, 40°44'52" N 127 m	Quartz, alkali feldspar	Zircon, titanite, Fe-Ti oxides
Yangjiazhangzi[6]	Granite porphyry	189.0–188.0	Premineralization	Yang 4	120°30'59" E, 40°49'22" N, 230 m	Quartz, alkali feldspar, plagioclase, biotite	Zircon, Fe-Ti oxides
Yangjiazhangzi	Granite porphyry	No data	Synmineralization	Yang 5	120°30'39" E, 40°49'06" N 208 m	Quartz, alkali feldspar, plagioclase, biotite	Zircon, Fe-Ti oxides
Yangjiazhangzi	Rhyolite porphyry	No data	Synmineralization	Yang 1, Yang 2	120°30'39" E, 40°49'06" N 208 m	Quartz, alkali feldspar, plagioclase, biotite	Zircon, titanite, Fe-Ti oxides

Age data from:
[1]Ma et al. (2013)
[2]Zhai et al. (2014)
[3]Zheng et al. (2014)
[4]Chu et al. (2017)
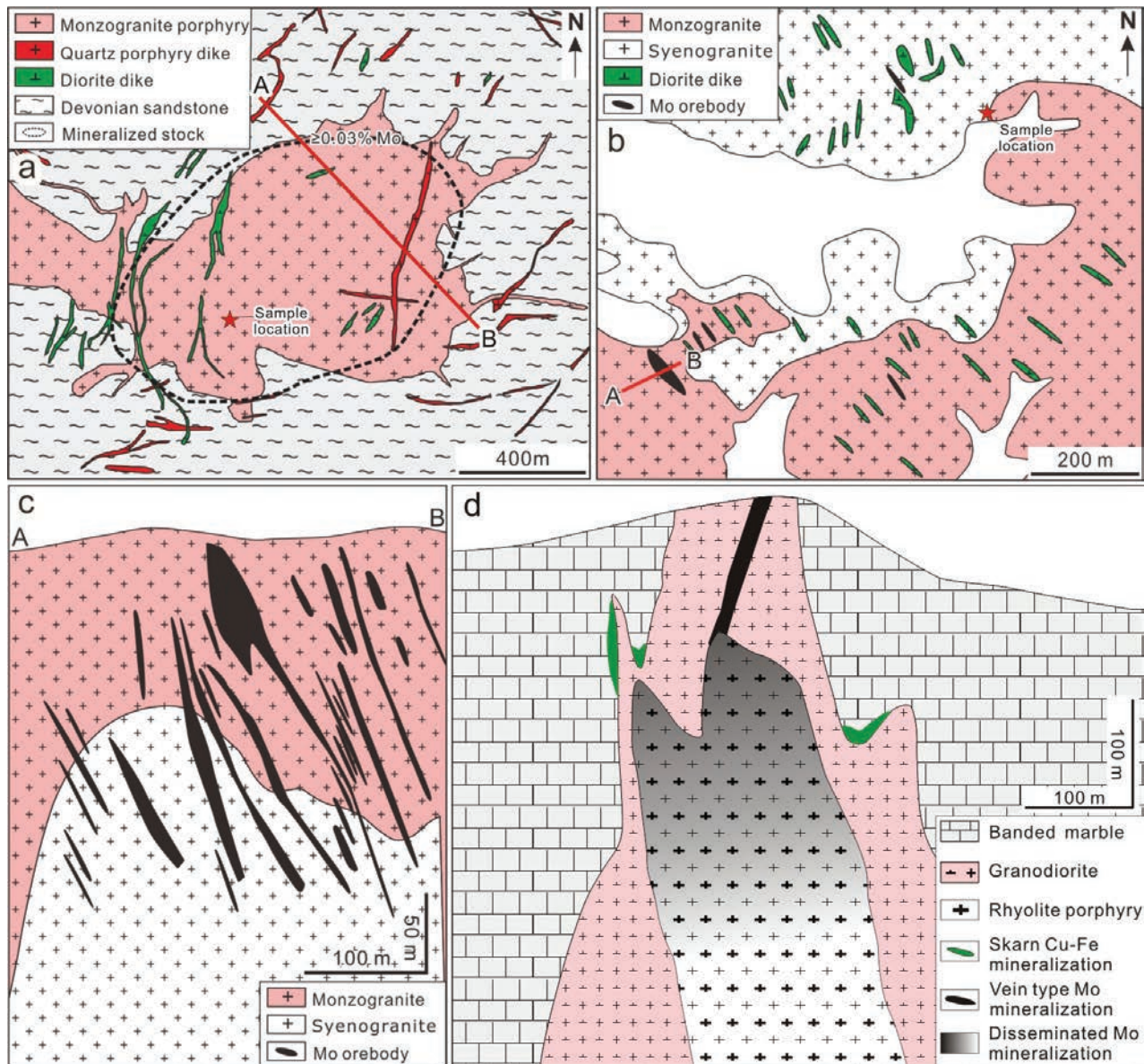[5]Yang et al. (1989)
[6]Wu et al. (2006)

Fig. 5. (a) Simplified geologic map of Aolunhua (Ma et al., 2013). (b) Simplified geologic map of Hashitu (Zhai et al., 2018). (c) Cross section along the marked line in (b) (Zhai et al., 2018). (d) Schematic cross section of Wanbaoyuan (Song et al., 2010).

monzogranite porphyry (Aolu 11, Fig. 6a), collected from the open pit, proved appropriate for melt inclusion work.

Hashitu Mo deposit

Hashitu is located ~50 km northwest of Aolunhua (Fig. 1). The deposit contains an indicated resource of 0.13 Mt Mo at an average grade of 0.13% (Zhai et al., 2018). Orebodies are hosted by monzogranite and syenogranite (Fig. 5b, c). Monzogranite varies from coarse equigranular to porphyritic and is exposed in the southern part of the deposit, where it covers an area of ~8 km² (Fig. 5b). It was cut by quartz-molybdenite ± pyrite veins with sericite and chlorite alteration halos (Zhai et al., 2018), sourced from the synmineralization intrusion (Fig. 5c), suggesting that monzogranite was emplaced prior to mineralization. The syenogranite has a sharp intrusive

contact with the monzogranite (Fig. 5c) and crops out mainly in the northern part of the deposit. It contains quartz veins with K-feldspar envelopes (Zhai et al., 2018) and is therefore interpreted to be a synmineralization intrusion. Zircon U-Pb dating returned an age of 147.0 ± 1.0 Ma for monzogranite and an age of 143.0 ± 2.0 Ma for syenogranite (Zhai et al., 2014). Diamond drilling has revealed two other synmineralization phases of rhyolite porphyry and granite porphyry at depth, which intruded the monzogranite and were in turn cut by quartz and molybdenite veins (Fig. 3e, f). The synmineralization phases at Hashitu have similar major and trace element compositions (SiO_2 = 76–77 wt %, K_2O = 4.6–5.8 wt %, A/CNK = 0.9–1.0, La_N/Yb_N = 3.2–9.7, δEu = 0.02–0.12; Zhai et al., 2014; this study) and Nd isotope values ($\varepsilon_{Nd}(t)$ = 1.1–2.1; Ding et al., 2016). Two drill core samples of premineralization
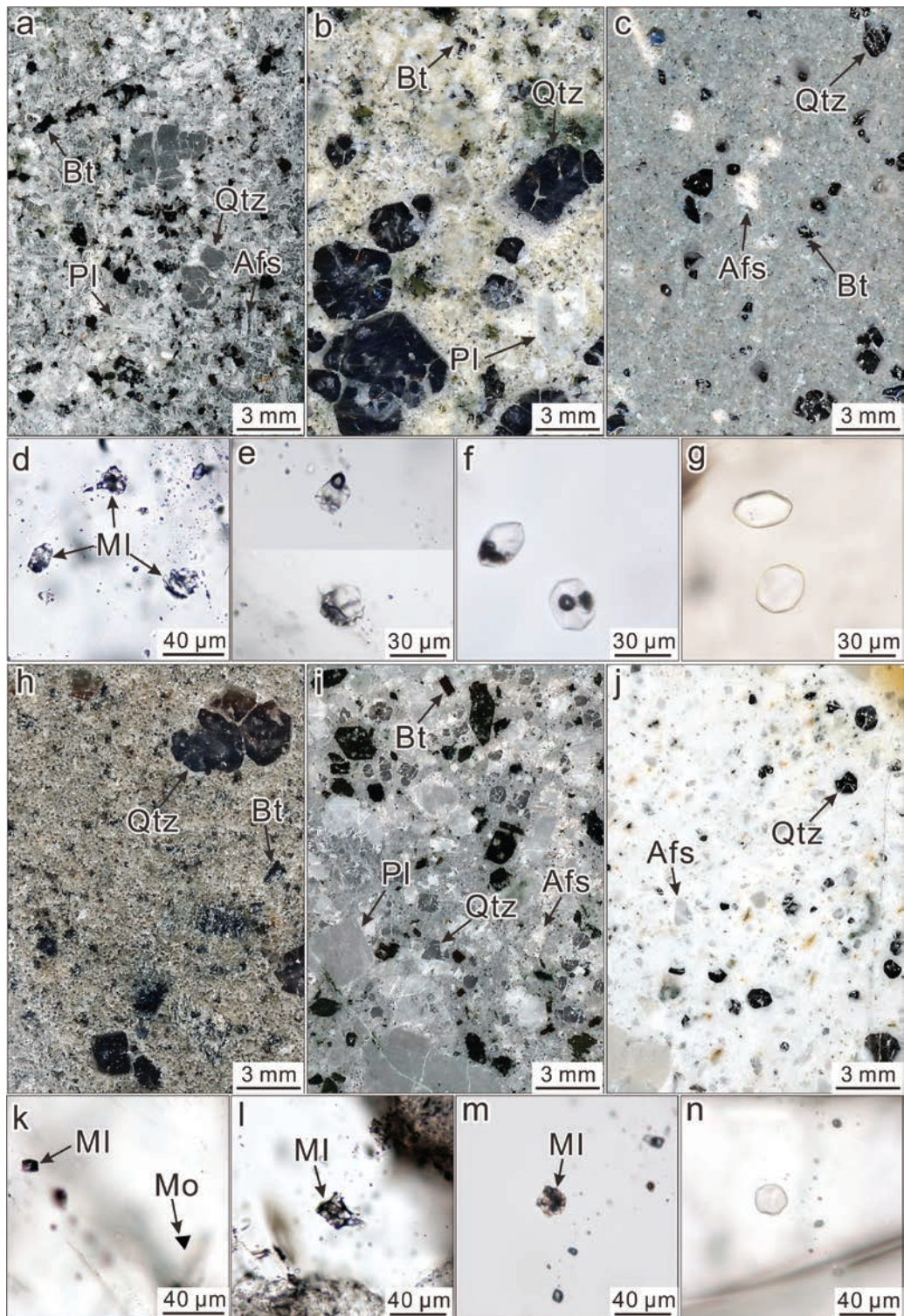
Fig. 6. Photographs of polished thick sections and melt inclusions in quartz phenocrysts. (a) Aolunhua monzogranite porphyry sample Aolu 11. (b) Hashitu porphyritic monzogranite sample Hash 10. (c) Hashitu rhyolite porphyry sample Hash 6. (d) Coarsely crystallized melt inclusion in sample Aolu 11. (e) Coarsely crystallized melt inclusions in Hash 10. (f) Partly crystallized melt inclusions in Hash 6. (g) The same melt inclusions as in (f), after homogenization at 2.0 kbar and 780°C in a rapid-quench cold-seal pressure vessel. (h) Hashitu granite porphyry sample Hash 5. (i) Wanbaoyuan granodiorite sample Wan 10. (j) Wanbaoyuan rhyolite porphyry sample Wan 1. (k) Coarsely crystallized melt inclusion coexisting with triangular, semitransparent molybdenite crystal in sample Hash 5. (l) Coarsely crystallized melt inclusion in sample Wan 10. (m) Finely crystallized melt inclusion in sample Wan 1. (n) The same melt inclusions as in (m), after homogenization at 2.0 kbar and 780°C in a rapid-quench cold-seal pressure vessel. Abbreviations: Afs = alkali feldspar, Bt = biotite, Hbl = hornblende, MI = melt inclusion, Mo = molybdenite, Pl = plagioclase, Qtz = quartz.

monzogranite (Hash 10 and Hash 13, Fig. 6b), two samples of synmineralization rhyolite porphyry (Hash 6 and Hash 7, Fig. 6c), and one sample of synmineralization granite porphyry (Hash 5, Fig. 6h) contained workable melt inclusions.

Wanbaoyuan Mo deposit

Wanbaoyuan is located in the eastern part of the North China craton, near the boundary between China and North Korea (Fig. 1b). It has an indicated resource of 0.12 Mt Mo at an average grade of 0.12% (Hu et al., 2007). Mineralization produced molybdenite-quartz veins (1–2 cm in width) in granodiorite and molybdenite veinlets (1–1.5 mm in width) in rhyolite porphyry (Song et al., 2010; Figs. 3h, 5d). The granodiorite is the oldest and largest intrusion, covering an area of ~126 km^2 (Song et al., 2010). Zircon U-Pb dating of granodiorite yielded an age of 130.0 ± 0.4 Ma (Yang et al., 1989). In the mining area, granodiorite was intruded by synmineralization rhyolite porphyry, which contains quartz veins with K-feldspar and biotite envelopes (Song et al., 2010) and molybdenite veinlets (Fig. 3h), and was cut by chalcopyrite veinlets with sericite alteration halos (Fig. 3g), indicating that granodiorite is a premineralization intrusion. Small lamprophyre and diorite dikes, which are contemporaneous with rhyolite porphyry (Hu et al., 2007; App. Fig. S2), occur in the southeastern part of the deposit. The granodiorite has SiO$_2$ contents of 63 to 66 wt % and K$_2$O contents of 3.7 to 3.9 wt %, and it is metaluminous (A/CNK = 0.9–1.0; App. Table S1). It is characterized by strong fractionation between LREEs and HREEs (La$_N$/Yb$_N$ = 9.4–18.7), a negligible Eu anomaly (δEu = 0.9–1.0), and high Sr/Y ratios (38–41). The rhyolite porphyry is rich in silica (SiO$_2$ = 74–78 wt %) and K$_2$O (5.7–6.6 wt %) and is peraluminous (A/CNK = 1.1–1.7). It is characterized by only a slight fractionation between LREEs and HREEs (La$_N$/Yb$_N$ = 0.6–0.9) and a strong negative Eu anomaly (δEu = 0.03–0.06). One sample of premineralization granodiorite (Wan 10, Fig. 6i) and three samples of synmineralization rhyolite porphyry (Wan 1, Wan 2, and Wan 3, Fig. 6j) collected from the underground mine proved suitable for melt inclusion analyses.

Methods

Doubly polished thin sections of 0.3- to 0.5-mm thickness were prepared from each sample and subsequently examined with a standard petrographic microscope, with a focus on melt inclusions and mineral inclusions occurring within quartz phenocrysts. Selected phenocrysts and melt inclusions were analyzed by laser ablation-inductively coupled plasma-mass spectrometry (LA-ICP-MS) or were rehomogenized and subsequently analyzed by electron probe microanalysis (EPMA).

Major and trace elements in nonhomogenized, unexposed melt inclusions were analyzed with a 193-nm ArF Excimer laser ablation system coupled to a PerkinElmer Elan DRC-e quadrupole ICP-MS at the Bayerisches Geoinstitut. The laser was operated at 5 to 10 Hz and an energy density of 3 to 10 J/cm^2 at the sample surface. The sample chamber was flushed with He gas at a rate of 0.4 l/min, to which 5 ml/min H$_2$ gas was added on the way to the ICP-MS system (Guillong and Heinrich, 2007). The ICP-MS system was tuned to a ThO rate of 0.07 ± 0.02% and a rate of doubly charged Ca ions of 0.10 ± 0.03% based on measurements on NIST SRM 610 glass. Measured elements include ^{7}Li, ^{11}B, ^{23}Na, ^{25}Mg, ^{27}Al,

^{30}Si, ^{39}K, ^{42}Ca, ^{49}Ti, ^{55}Mn, ^{57}Fe, ^{65}Cu, ^{85}Rb, ^{88}Sr, ^{89}Y, ^{90}Zr, ^{93}Nb, ^{98}Mo, ^{118}Sn, ^{133}Cs, ^{137}Ba, ^{140}Ce, ^{184}W, ^{208}Pb, ^{209}Bi, and ^{238}U, using dwell times of 10 to 40 ms per isotope. NIST SRM 610 was used as an external standard and was analyzed twice at the beginning and the end of each block of up to 20 analyses. A well-characterized in-house obsidian standard was analyzed in each session as an unknown to check the accuracy of the analyses. A beam diameter of 40 μm was used for glasses, whereas for melt inclusions the size of the beam was adjusted to ensure ablation of the entire melt inclusion but at the same time keep the amount of ablated host mineral to a minimum. Before each melt inclusion analysis, the quartz host was analyzed nearby in order to get a clean and sufficiently long signal that could be used for Ti-in-quartz (TitaniQ) thermobarometry.

Entire, unexposed melt inclusions were ablated by means of a pulsed laser beam out of the surrounding quartz host and any excess ablated host was subtracted numerically from the resulting LA-ICP-MS signals until constraints from whole-rock compositional data (for use as internal standard) were met (Halter et al., 2002). A total of 118 melt inclusions were analyzed. Internal standardization of the melt inclusions from Aolunhua, Yangjiazhangzi, Lanjiagou, and Songbei was based on SiO$_2$ vs. Al$_2$O$_3$ trends defined by corresponding whole-rock data published in Ma et al. (2013), Wu et al. (1990), Chu et al. (2017), and in the present study (App. Table S1). For the melt inclusions from Hashitu and Wanbaoyuan, fixed Al$_2$O$_3$ contents of 11.5 and 12.0 wt %, respectively, were used based on whole-rock data and EPMA analyses of rehomogenized melt inclusions (App. Tables S1, S2). Because quartz-hosted melt inclusions tend to lose Na during postentrapment melt crystallization (Zajacz et al., 2009; Audétat and Lowenstern, 2014), estimates regarding their original Na$_2$O contents had to be made. Based on whole-rock data and EPMA analyses, a value of 4.0 wt % Na$_2$O was chosen for Aolunhua, Yangjiazhangzi, Lanjiagou, and Songbei, whereas for Hashitu and Wanbaoyuan a value of 3.5 wt % Na$_2$O was chosen. The sum of the major element oxides of melt inclusions was then normalized to 100 wt %—i.e., the analyses are reported dry. Uncertainties associated with these analyses are estimated at 5 to 7%, except for elements close to the detection limit.

LA-ICP-MS analyses of the host quartz were quantified based on NIST SRM 610 as an external standard and normalizing the sum of all major element oxides to 100 wt %. The accuracy of these analyses was checked periodically by means of the quartz standard described in Audétat et al. (2015).

A total of 48 unexposed melt inclusions in quartz phenocrysts from the ore-related intrusions at Hashitu, Wanbaoyuan, and Yangjiazhangzi were rehomogenized and then analyzed by EPMA at the Bayerisches Geoinstitut. For this purpose, melt inclusion-bearing quartz fragments of ~2- × 2- × 0.5-mm size were cut out of the polished sections and placed in an open Pt capsule in the top of a vertically operated titanium-zirconium-molybdenum (TZM) cold-seal pressure vessel, where the melt inclusions were rehomogenized at 1.5 to 2.0 kbar, confining Ar pressure in one step of four days' duration at 780°C. The runs were terminated by dragging the samples with the help of a magnet from the hot end to the cold end of the pressure vessel within ~20 s. After this treatment, most melt inclusions were found to be fully rehomogenized and quenched to silicate glass, but some

larger inclusions remained heterogeneous and contained a vapor bubble ± small crystals, probably in response to slow melting kinetics. Quartz fragments were polished by hand to expose fully rehomogenized inclusions on the sample surface for subsequent analysis by EPMA. These analyses were performed on a JEOL JXA-8200 microprobe equipped with five spectrometers and TAP, PET, LiF, and LDE1 spectrometer crystals, using 15 kV, 20 nA, and a beam defocused to 10 μm. Sodium, K, Si, S, and Fe were measured first, with Na and K being measured for 10 s on peak and 5 s on each background ($10/2 \times 5$), and Si, Al, Ti, Fe, Mn, Mg, and Ca with $20/2 \times 10$, and F, Cl, and S with $60/2 \times 30$. Time-resolved signals showed up to 10% loss of Na in the most hydrous glasses, but no loss of Cl and F. Standardization was performed on albite (Na, Si), orthoclase (K), spinel (Al), $MnTiO_3$ (Mn, Ti), metallic Fe, enstatite (Mg), wollastonite (Ca), fluorite (F), vanadinite (Cl), and barite (S). A topaz crystal that contains 20.5 ± 0.5 wt % F according to X-ray diffraction measurements and the equations for cell parameters *a* and *b* given by Alberico et al. (2003) was measured as an unknown. It returned F values of 20.1 ± 0.2 wt %. Rough estimates of water contents were obtained by taking the difference to 100 wt % total and correcting it for the abundance of F. However, owing to uncertainties in the homogenization procedure and the EPMA analyses themselves (e.g., Devine et al., 1995; Donovan and Vicenzi, 2008), these values are associated with an error of at least ±1 wt %.

Results

Yangjiazhangzi

Representative LA-ICP-MS analyses of melt inclusions from Yangjiazhangzi are listed in Table 2, whereas the full dataset of 25 melt inclusions is provided in Appendix Table S3. Melt inclusions in the premineralization intrusion are crystallized (Fig. 4d) and contain ~80 wt % SiO_2, 350 to 440 ppm Rb, 5 to 11 ppm Cs, and 4 to 6 ppm Mo. They are thus distinctly more evolved than average granite (150 ppm Rb, 5 ppm Cs; Taylor, 1964), but are less evolved than mineralizing magmas of Climax-type Mo systems (300–1,000 ppm Rb, 10–30 ppm Cs; Lowenstern, 1994; Mercer et al., 2015; Audétat and Li, 2017; Figs. 7, 8).

Melt inclusions in synmineralization phases are mostly glassy and negative crystal shaped (Fig. 4e). They are rhyolitic in composition (79–80 wt % SiO_2) and contain significantly less Rb (mostly 180–220 ppm) and Cs (mostly 3–6 ppm) than those of the premineralization intrusion, suggesting a lower degree of melt fractionation. Molybdenum concentrations in the silicate melts show a narrow range of 2 to 4 ppm with an average value of 2 ppm, which is about two times less than in similarly evolved melts from Climax-type deposits (Fig. 8).

Representative EPMA analyses of 24 rehomogenized melt inclusions from synmineralization phases are provided in Table 3, and the full dataset is available in Appendix Table S2. Because many melt inclusions developed local decrepitation halos (e.g., Fig. 4d), only about half of the melt inclusions returned realistic Na_2O values (3.7–4.3 wt %), with the others containing either too little (2.0–3.1 wt %) or too much (4.6–5.4 wt %) Na_2O compared to whole rocks (3.6–4.4 wt % Na_2O; App. Table S1). The anomalous values were thus corrected to an Na_2O content of 4.0 wt % (based on the average

composition of the other inclusions). A few melt inclusions also showed unrealistic K_2O and Al_2O_3 concentrations and were therefore replaced by the average values present in the other inclusions (3.5 wt % for K_2O and 11.5 wt % for Al_2O_3, respectively). After these corrections and normalization to 100 wt % (i.e., dry composition), the rehomogenized melt inclusions gave values that agreed with the results obtained by LA-ICP-MS. The rehomogenized melt inclusions contain up to 0.05 wt % Cl, 0.07 wt % S (expressed as SO_3), and 4.6 to 7.4 wt % H_2O (with a mode at 5.3–6.5 wt %, based on the difference from a total 100 wt %, corrected for O-F substitution), whereas F contents were always below the detection limit of ~0.15 wt % (App. Table S2).

Songbei

Melt inclusions in the synmineralization intrusion from Songbei are finely crystallized and partially decrepitated (in the upper part of Fig. 4i), and they range in size from 14 to 60 μm. The melt inclusions are rhyolitic in composition (78–81 wt % SiO_2) and contain 140 to 1,300 ppm Rb (with a mode at 150–250 ppm) and 2 to 88 ppm Cs (with a mode at 2–5 ppm; App. Table S3). The wide range of incompatible element concentrations indicates that the melts were trapped under varied degrees of magma fractionation. However, Mo concentrations in the silicate melts are relatively constant at 3 ± 1 ppm, which is at the lower end of the range observed in barren and Climax-type ore deposits at this degree of melt fractionation (Fig. 8).

Lanjiagou

Melt inclusions in the synmineralization sample from Lanjiagou are finely crystallized (in the lower part of Fig. 4i) and measure up to 45 μm in size. Because they are sparse and relatively poorly preserved, only two were analyzed. The analyzed melt inclusions contain 78 to 79 wt % SiO_2, 220 to 340 ppm Rb, 2 to 8 ppm Cs, and 4 to 5 ppm Mo (App. Table S3) and are thus slightly more evolved than average granite.

Aolunhua

Melt inclusions in the synmineralization sample from Aolunhua are coarsely crystallized and commonly surrounded by halos of tiny fluid inclusions (Fig. 6d). The analyzed melt inclusions are rhyolitic in composition (77–80 wt % SiO_2) and span a wide concentration range of compatible elements (50–320 ppm Sr and 56–800 ppm Ba) and incompatible elements (70–280 ppm Rb, with a mode at 200–250 ppm Rb, and 1–16 ppm Cs, with a mode at 5–10 ppm Cs). The low Mo concentrations in the melt inclusions are similar to those in the deposits described above, ranging from 1 to 3 ppm (App. Table S3).

Hashitu

Melt inclusions in premineralization phases from Hashitu are coarsely crystallized (Fig. 6e). They contain, on average, 80 wt % SiO_2, plus 300 to 650 ppm Rb (with a mode at 300–420 ppm) and 5 to 48 ppm Cs (with a mode at 10–28 ppm). Molybdenum concentrations range from 1 to 5 ppm, with an average of 3 ppm.

Melt inclusions in synmineralization phases from Hashitu are either finely crystallized or glassy and are rarely intergrown with molybdenite inclusions (Fig. 6f, k). They are

Table 2. Representative Compositions of Melt Inclusions Analyzed in This Study

Deposit	Aolunhua		Hashitu		Lanjiagou		Songbei		Wanbaoyuan		Yangjiazhangzi	
Rock unit	Monzogranite porphyry		Rhyolite porphyry		Fine-grained syenogranite		Rhyolite porphyry		Rhyolite porphyry		Rhyolite porphyry	
Sample no.	Aol 11 MI2	Aol 11 MI	Hash 6 MI	Hash 7 MI2	Lanji 7 MI1	Lanji 7 MI2	Song1 MI2	Song1 MI3	Wan 1 MI	Wan 2 MI2	Yang 2 MI1	Yang 2 MI2
Major elements (wt %)												
SiO_2	79.2	79.1	79.2	79.4	79.3	77.8	79.6	79.3	79.3	79.0	79.3	79.8
TiO_2	0.09	0.09	0.06	0.06	0.12	0.07	0.10	0.09	0.06	0.06	0.05	0.06
Al_2O_3	12.1	12.1	11.5	11.5	11.8	11.9	11.8	11.8	12.0	12.0	11.8	11.8
FeO	0.54	0.56	0.73	0.77	0.87	0.41	0.52	0.48	0.41	0.40	0.43	0.46
MgO	0.05	0.04	0.01	0.01	0.34	0.03	0.04	0.04	0.03	0.03	0.04	0.04
MnO	0.01	0.01	0.02	0.02	0.01	0.01	0.03	0.03	0.05	0.05	0.05	0.04
CaO	1.04	1.11	0.37	0.53	0.04	0.38	0.42	0.59	0.55	0.58	0.75	0.65
Na_2O[1]	3.9	3.9	4.1	3.8	3.8	3.8	3.9	3.6	3.9	3.9	3.4	3.8
K_2O	3.1	3.0	4.0	4.0	3.7	5.5	3.5	4.1	3.7	4.0	4.1	3.3
Total[2]	100.0	100.0	100.0	100.0	100.0	100.0	100.0	100.0	100.0	100.0	100.0	100.0
Trace elements ($\mu g/g$)												
Li	30	16	130	100	<14	<2	5	4	9	<2	45	18
B	48	37	22	13	<15	5	13	10	110	120	21	24
Cu	<7	<2	8	11	<7	<2	10	9	4	5	<4	1
Cs	210	210	210	200	340	220	180	170	180	230	190	220
Mo	65	72	3	2	30	35	6	9	8	8	43	50
Y	10	12	33	32	14	10	9	10	14	15	7	7
Nb	68	70	140	140	50	69	37	65	52	52	56	55
Rb	6	6	12	12	20	17	21	19	20	24	15	16
Sr	3	2	1	1	5	4	4	3	5	2	3	3
Zr	<12	<4	6	5	<15	<3	<2	2	<3	<4	<5	<1
Sn	6	8	9	8	8	2	3	3	6	7	4	5
Ba	200	100	6	3	8	10	15	21	14	12	130	120
Ce	39	56	61	59	<2	30	41	38	25	33	24	22
W	<4	1	2	1	<4	1	2	1	2	<1	1	1
Pb	8	8	26	24	<2	14	16	14	32	32	16	26
Bi	1	<1	1	0	<1	0	0	0	0	0	0	0
U	3	3	6	6	3	13	2	4	6	7	3	3

[1] Estimated based on whole-rock composition
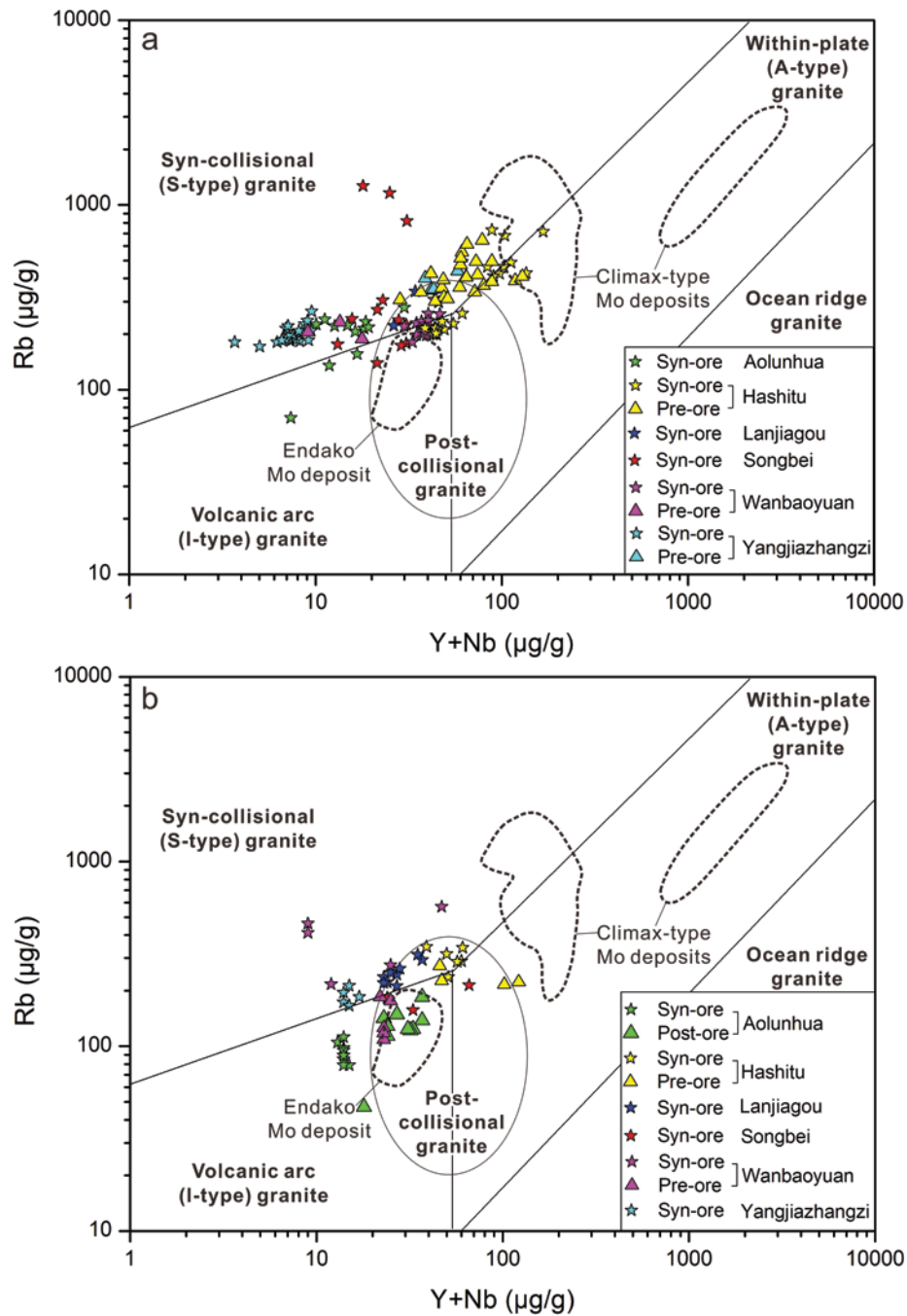[2] On a volatile-free basis; sample locations are the same as in Table 1

Fig. 7. Trace element signatures of (a) melt inclusions and (b) whole rocks of the present study, plotted on the tectonic discrimination diagram of Pearce et al. (1984) and Pearce (1996). The trace element signatures of melt inclusions analyzed from Climax-type deposits (Lowenstern, 1994; Audétat, 2010, 2015; Audétat et al., 2011; Mercer et al., 2015; Audétat and Li, 2017; Zhang and Audétat, 2017) and of whole rocks associated with Endako Mo deposit (Whalen et al., 2001) are shown for comparison.

geochemically similar to the premineralization melt inclusions, containing 79 to 81 wt % SiO_2, 200 to 730 ppm Rb (with a mode at 200–500 ppm), 8 to 53 ppm Cs (with a mode at 10–24 ppm), and 1 to 7 ppm Mo (3 ppm, on average; App. Table S3). The presence of molybdenite inclusions in quartz phenocryst suggests that this magma was at least temporarily molybdenite saturated. However, the rarity of the molybdenite inclusions and the fact that the Mo content of the silicate melt generally increases with increasing degree of melt fractionation (monitored by Rb or Cs; Fig. 8) suggest that only minor molybdenite precipitated.

Seventeen melt inclusions from synmineralization phases were rehomogenized for EPMA. The rehomogenized melt inclusions contain 4.4 to 7.8 wt % H_2O (with a mode at 5.0–7.0 wt %), up to 0.4 wt % F, 0.03 to 0.09 wt % Cl, and ≤0.02 wt % S (App. Table S2).
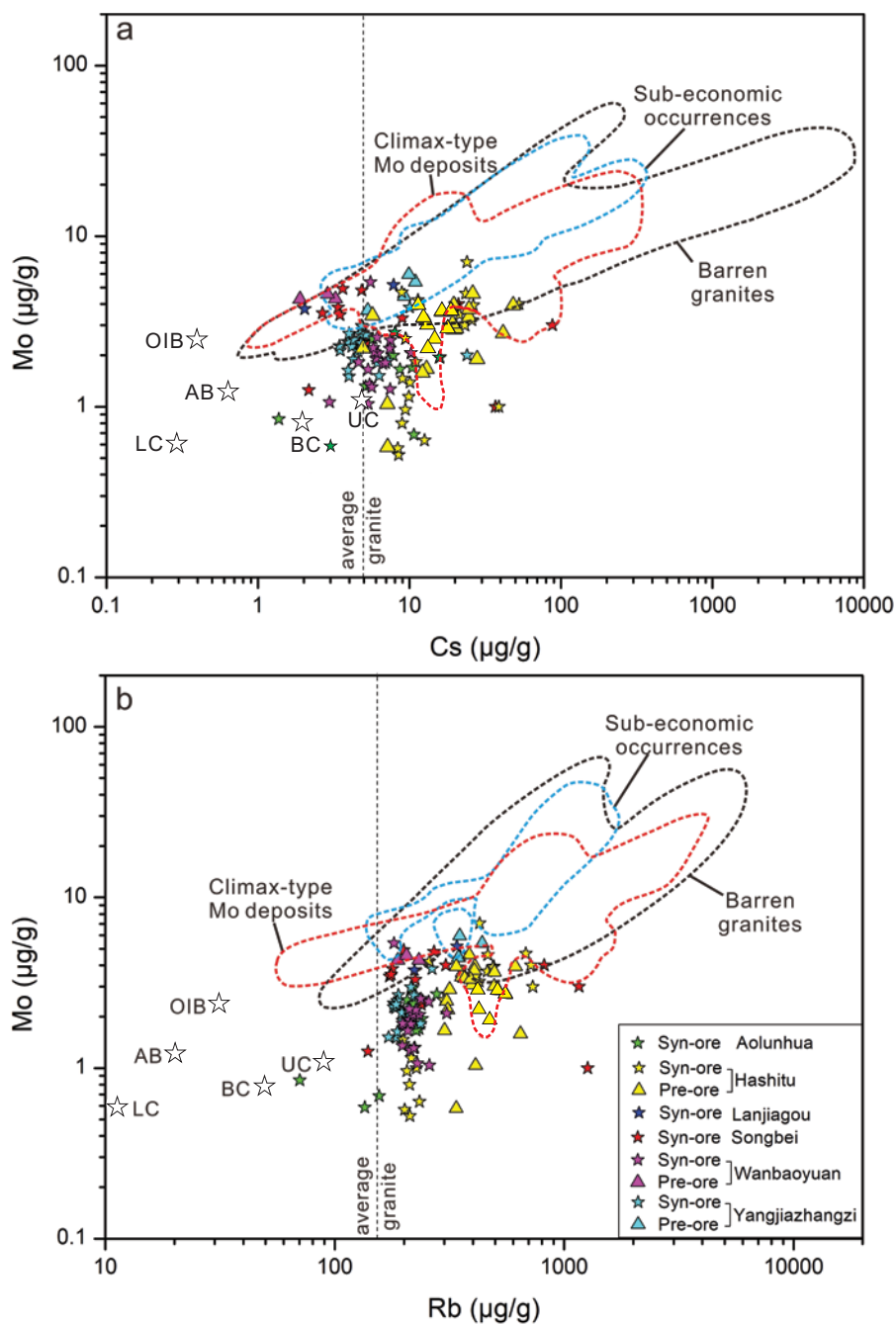
Fig. 8. Molybdenum concentrations vs. (a) Cs concentrations and (b) Rb concentrations in melt inclusions analyzed in the present study. The Mo, Cs, and Rb concentrations in melt inclusions analyzed from Climax-type porphyry Mo deposits (Lowenstern, 1994; Audétat, 2010, 2015; Audétat et al., 2011; Mercer et al., 2015; Audétat and Li, 2017; Zhang and Audétat, 2017), subeconomic occurrences with affinity to Climax-type deposits (Audétat, 2010; Lerchbaumer and Audétat, 2013; Audétat and Li, 2017), and barren granites (Audétat and Pettke, 2003; Audétat et al., 2008; Lerchbaumer and Audétat, 2013) are shown for comparison. The Cs and Rb contents of average granite are taken from Taylor (1964). Abbreviations: AB = average composition of primitive arc basalts (GEOROC database; references given in Bali et al., 2012); LC, BC, UC = average composition of lower crust, bulk crust, and upper crust, respectively (Rudnick and Gao, 2003); OIB = average composition of oceanic island basalts (Sun and McDonough, 1989).

Wanbaoyuan

Melt inclusions in the premineralization intrusion from Wanbaoyuan are finely crystallized, have irregular shapes, and are commonly surrounded by halos of tiny fluid inclusions (Fig. 5l). The analyzed melt inclusions are rhyolitic in composition (77–79 wt % SiO$_2$) and are relatively rich in compatible elements (42–58 ppm Sr and 350–380 ppm Ba) and low in Cs (2–3 ppm), but still contain more Rb (190–230 ppm) than average granite. The Mo concentration in these melt inclusions is 4 to 5 ppm (App. Table S3), which

Table 3. Representative Electron Microprobe Analyses of Rehomogenized Melt Inclusions

Analysis	SiO₂	Na₂O	K₂O	FeO	MgO	CaO	MnO	Al₂O₃	TiO₂	SO₃	F	Cl	Total	O=F	H₂O[1]
Hashitu deposit, synmineralization rhyolite porphyry (Hash 6, Hash 7)															
Ha 6d 1	74.71	3.74	2.72	0.71	0.03	0.51	0.05	11.16	0.04	0.01	0.34	0.03	94.04	0.14	6.11
Ha 6d 2	74.71	3.69	2.63	0.69	0.03	0.51	0.05	11.24	0.05	0.01	0.38	0.04	94.03	0.16	6.13
Ha 6d 6	74.53	4.08	3.89	0.86	0.01	0.47	0.02	11.24	0.02	0.02	0.29	0.06	95.50	0.12	4.62
Ha 6d 7	73.68	3.55	3.84	0.76	0.02	0.44	0.02	11.17	0.06	0.02	0.39	0.08	94.02	0.17	6.14
Ha 6a 1	74.67	3.86	4.01	0.70	0.01	0.44	0.01	11.63	0.09	0.01	0.27	0.07	95.76	0.11	4.35
Ha 6a 4	73.22	3.46	4.05	0.68	0.01	0.44	0.01	11.29	0.06	0.01	0.14	0.08	93.44	0.06	6.62
Ha 7a 1	71.35	3.51	3.87	0.74	0.01	0.47	0.03	11.86	0.06	b.d.	0.33	0.08	92.31	0.14	7.83
Ha 7a 2	74.79	3.62	3.69	0.39	0.04	0.53	0.05	10.41	0.04	0.02	b.d.	0.03	93.61	0.00	6.39
Ha 7a 3	75.12	3.53	3.61	0.38	0.04	0.55	0.03	10.37	0.06	0.01	b.d.	0.03	93.73	0.00	6.27
Ha 7a 4	75.21	3.48	3.66	0.35	0.03	0.53	0.04	10.48	0.06	b.d.	b.d.	0.04	93.89	0.00	6.11
Wanbaoyuan, synmineralization rhyolite porphyry (Wan 1, Wan 2)															
Wan 2d 1	76.59	4.14	3.57	0.38	0.03	0.40	0.07	10.70	0.08	b.d.	b.d.	0.04	96.00	0.00	4.00
Wan 2d 2	76.39	4.11	3.62	0.39	0.03	0.37	0.06	10.78	0.04	b.d.	b.d.	0.04	95.83	0.00	4.17
Wan 1b 1	75.35	4.77	3.48	0.38	0.04	0.40	0.04	10.99	0.06	b.d.	b.d.	0.05	95.58	0.00	4.42
Wan 1b 2	75.36	4.23	3.63	0.37	0.03	0.34	0.05	11.47	0.05	0.01	b.d.	0.03	95.59	0.00	4.41
Wan 1g 1	75.66	3.85	4.20	0.39	0.02	0.22	0.04	11.45	0.06	0.02	b.d.	0.05	95.96	0.00	4.04
Yangjiazhangzi, synmineralization rhyolite porphyry (Yang 1, Yang 2)															
Yang 1f 2	74.11	4.14	3.62	0.40	0.03	0.53	0.05	11.08	0.06	0.01	b.d.	0.01	94.04	0.00	5.96
Yang 2c 3	75.12	4.27	3.34	0.38	0.02	0.50	0.06	10.68	0.05	b.d.	b.d.	0.02	94.44	0.00	5.56
Yang 2c 4	75.36	3.91	3.35	0.40	0.04	0.54	0.03	10.56	0.03	b.d.	b.d.	0.02	94.25	0.00	5.75
Yang 2e 3	74.20	4.32	3.40	0.42	0.04	0.56	0.03	10.85	0.06	b.d.	b.d.	0.04	93.91	0.00	6.09
Yang 2e 5	74.27	4.03	3.54	0.41	0.03	0.55	0.04	10.52	0.02	0.03	b.d.	0.03	93.47	0.00	6.53
Yang 2e 7	73.84	3.90	3.44	0.39	0.04	0.51	0.05	10.67	0.06	0.02	b.d.	0.03	92.96	0.00	7.04
Yang 2b 1	75.15	3.89	3.49	0.39	0.04	0.53	0.06	10.63	0.06	b.d.	b.d.	0.03	94.26	0.00	5.74
Yang 2b 2	75.57	4.28	3.20	0.39	0.02	0.54	0.04	10.39	0.06	0.02	b.d.	0.05	94.56	0.00	5.44
Yang 2b 4	74.81	4.60	3.31	0.37	0.02	0.55	0.04	10.48	0.05	0.02	b.d.	0.03	94.28	0.00	5.72
Yang 2a 4	74.37	3.70	2.15	0.55	0.06	1.36	0.04	11.54	0.09	0.02	b.d.	b.d.	93.87	0.00	6.13

Notes: Sample locations are the same as in Table 1; all data are in wt %; b.d. = below detection
[1] Estimated based on the difference to 100 wt %

is slightly lower than values of similarly evolved melts from Climax-type deposits (Fig. 8).

Melt inclusions in the synmineralization intrusion are finely crystallized, have rounded shapes (Fig. 6m), and could be completely rehomogenized (Fig. 6n). They contain ~79 wt % SiO_2 and ~7.8 wt % total alkalis ($Na_2O + K_2O$; App. Table S3). In terms of trace element compositions, they record a higher degree of fractionation than the melts from the premineralization phase, as they contain 1 to 12 ppm Sr, 5 to 15 ppm Ba, and 3 to 10 ppm Cs (the latter with a mode at 5–7 ppm). The Rb concentrations (180–310 ppm; with a mode at 200–240 ppm), however, are approximately the same. The Mo concentration in these melt inclusions is 1 to 5 ppm.

Seven melt inclusions from the synmineralization phase were rehomogenized for EPMA, but three analyses returned unreasonable Na_2O values. After correcting the Na_2O content to 4.0 wt % and normalizing the total to 100 wt %, the rehomogenized melt inclusions contain 4.0 to 5.2 wt % H_2O and 0.03 to 0.05 wt % Cl, whereas S contents were ≤0.02 wt % and F contents were always below the detect limit of 0.15 wt % (App. Table S2).

In summary, all melt inclusions analyzed from the six investigated porphyry Mo deposits in northeast China are rhyolitic in composition. The least-evolved melt inclusions, which approach the composition of the bulk magmas, contain 2 to 11 ppm Cs and 150 to 390 ppm Rb, suggesting that they are one to two times more evolved than average granite. An exception is the melts from Hashitu, which contain 10 to 28 ppm Cs and 200 to 500 ppm Rb and, thus, are about three to four times more evolved than average granite. Molybdenum concentrations were generally rather low in the melts of both pre- and synmineralization intrusions, with most values falling between 1 and 7 ppm. Fluorine concentrations are below the detection limit of ~0.15 wt % in all deposits except for Hashitu, where melts containing up to 0.4 wt % F were found. Water contents are high in the synmineralization intrusions of Hashitu and Yangjiazhangzi (with a mode at 5.0–7.0 wt %) and slightly lower (4.0–5.2 wt % H_2O) at Wanbaoyuan.

Reconstruction of Magmatic P-T-f_{O_2} Conditions

To reconstruct the crystallization conditions of the mineralizing magmas, the following methods were used: (1) zircon saturation thermometry (Watson and Harrison, 1983), (2) TitaniQ thermobarometry (Huang and Audétat, 2012; Audétat, 2013), and (3) oxygen fugacity estimates based on molybdenite saturation (Audétat et al., 2011; Sun et al., 2014). The results are summarized in Table 4, and the full data set is available in Appendix Table S3.

All analyzed melt inclusions in quartz are metaluminous to peraluminous in composition and have been saturated in zircon, as demonstrated by the common presence of zircon inclusions within the quartz phenocrysts, thus permitting use of the zircon saturation thermometer of Watson and Harrison (1983). The results obtained for Aolunhua, Lanjiagou, Wanbaoyuan, and Yangjiazhangzi are mostly between 730° and 690°C, whereas the melt inclusions from the synmineralization intrusion of Songbei returned slightly higher temperatures of 760° to 720°C (Table 4). Interestingly, the temperatures obtained from the premineralization intrusions at Wanbaoyuan and Yangjiazhangzi are, on average, slightly higher than those

obtained from the corresponding synmineralization intrusions (770°–690°C vs. 720°–690°C at Wanbaoyuan; 790°–730°C vs. 720°–690°C at Yangjiazhangzi), which points to the input of new magma prior to mineralization. In view of the considerable F contents of some melt inclusions from Hashitu (up to 0.4 wt % F), we calculated two zircon saturation temperatures for each inclusion: one assuming zero fluorine content and one assuming 0.4 wt % F. The latter was calculated based on the model of Keppler (1993) to account for the strongly enhanced Zr solubility in fluorine-bearing melts. Consequently, Zr concentrations of the melt inclusions from the Hashitu deposit are lowered by 8%, resulting in a temperature decrease of 7° to 9°C. Fluorine-corrected melt temperatures for the premineralization phases range from 770° to 670°C (with a mode at 760°–730°C), similar to those of the synmineralization intrusions (range from 780°–710°C, with a mode at 770°–740°C).

The TitaniQ approach described by Huang and Audétat (2012) and Audétat (2013) to reconstruct the pressures of quartz phenocryst crystallization uses the composition of melt inclusions next to the analyzed quartz to derive the temperature and the activity of TiO_2 in the magma. The latter was calculated based on the TiO_2 solubility model of Kularatne and Audétat (2014). For Hashitu, both a value assuming zero fluorine and a value assuming 0.4 wt % F were calculated, the latter using experimental data of Aseri et al. (2015). Results for the synmineralization intrusions from Aolunhua, Lanjiagou, Songbei, Wanbaoyuan, and Yangjiazhangzi are similar, with most values falling within the range of 3.7 to 1.5 kbar, which is comparable with the results of the premineralization intrusions (4.1–2.1 kbar; Table 4). At Hashitu, pressures calculated with corrected TiO_2 activities and zircon saturation temperatures are slightly lower than the other deposits, with most values ranging from 2.0 to 1.0 kbar in the synmineralization intrusion and from 2.8 to 1.0 kbar in the premineralization intrusions (Table 4).

As discussed above, melt inclusions in the synmineralization intrusions from Hashitu, Yangjiazhangzi, and Wanbaoyuan contain between 5.0 and 7.0 wt %, 5.3 and 6.5 wt %, and 4.0 and 5.2 wt % H_2O, respectively. These water contents require minimum entrapment pressures of 2.6 to 1.4 kbar at Hashitu, 2.3 to 1.6 kbar at Yangjiazhangzi, and 1.6 to 1.0 kbar at Wanbaoyuan (Johannes and Holtz, 1996). Comparison of these pressures with those constrained via TitaniQ (2.0–1.0 kbar at Hashitu; mostly 3.7–1.5 kbar at the other localities) shows that the corresponding averages agree well at Hashitu and Yangjiazhangzi, whereas at Wanbaoyuan the calculated minimum saturation pressures are on average ~1 kbar lower (Table 4). This suggests that the ore-forming magmas at the former two localities were likely fluid saturated through most of their crystallization history.

The synmineralization granite porphyry sample from Hashitu was molybdenite saturated, as indicated by the occurrence of molybdenite inclusions of unambiguously primary origin within quartz phenocrysts (Fig. 6k). Applying the method of using the Mo content of molybdenite-saturated melts in conjunction with zircon saturation temperatures (Audétat et al., 2011; Sun et al., 2014) to estimate magmatic f_{O_2}, we obtain a value of ~0.7 log units above the quartz-fayalite-magnetite buffer (i.e., QFM + 0.7) for the ore-related magma of Hashitu. For the other five deposits, no estimate of f_{O_2} could be made because no molybdenite inclusions were found in the quartz phenocrysts.

Table 4. Composition and Properties of Silicate Melts in Fertile Versus Barren Magmas of the Present Study and in Climax-Type Mo Deposits

Deposit	Aolunhua	Hashitu	Hashitu	Lanjiagou	Songbei	Wanbaoyuan	Wanbaoyuan
Fertility	Fertile	Fertile	Barren	Fertile	Fertile	Fertile	Barren
Mo reserve	1.7 Mt	0.13 Mt		0.22 Mt	0.17 Mt	0.12 Mt	
Setting[1]	I	A-I	A-I	I	I	I	I
Mo ($\mu g/g$)	1–3 (avg. 2)	1–7 (avg. 3)	1–5 (avg. 3)	4–5 (avg. 4)	1–5 (avg. 3)	1–5 (avg. 2)	4–5 (avg. 4)
Rb ($\mu g/g$)	200–250	200–500	300–420	220–340	150–250	200–240	190–230
Cs ($\mu g/g$)	5–10	10–24	10–28	2–8	2–5	5–7	2–3
F (wt %)		≤0.4				<0.15	
Cl (wt %)		0.03–0.09				0.03–0.05	
S (wt %)		≤0.02				≤0.02	
H_2O (wt %)[2]		5.0–7.0				4.0–5.2	
Min. P (kbar)[3]		1.4–2.6 (avg. 2.0)				1.0–1.6 (avg. 1.3)	
T (°C)[4]	700–730	740–770	730–760	700–710	720–760	690–720	690–770
P (kbar)[5]	2.0–2.5 (avg. 2.3)	1.0–2.0 (avg. 1.5)	1.0–2.8 (avg. 1.9)	1.9	1.5–2.5 (avg. 2.1)	2.3–3.5 (avg. 2.5)	2.3–4.1 (avg. 3.5)
$\log \eta$ (Pa s)[6]		4.3–5.1				5.8–6.1	
$\log f_{O_2}$ (ΔFMQ)[7]		0.7					

Deposit	Yangjiazhangzi	Yangjiazhangzi	Urad-Henderson[8]	Silver Creek[9]	Climax[10]	Pine Grove[11]
Fertility	Fertile	Barren	Fertile	Fertile	Fertile	Fertile
Mo reserve	0.26 Mt		1.0 Mt	0.12 Mt	2.20 Mt	0.37 Mt
Setting[1]	I	I-A	A	A	A	A
Mo ($\mu g/g$)	2–4 (avg. 2)	4–6 (avg. 5)	10–25 (avg.19)	3–4 (avg. 3)	5–7 (avg. 6)	2–4 (avg. 3)
Rb ($\mu g/g$)	180–220	350–440	500–700	400–500	500–1,500	400–500
Cs ($\mu g/g$)	3–6	5–11	10–20	11–15	15–90	12–15
F (wt %)	<0.15		0.5–1.0	0.25–0.32	3.1–3.9	0.2–0.9
Cl (wt %)	≤0.05		0.21–0.35	0.04–0.05	0.06–0.12	0.04–0.12
S (wt %)	≤0.07				0.01–0.02	
H_2O (wt %)[2]	5.3–6.5		6.0–7.0	6.0–9.0	4.0–6.0	6.0–8.0
Min. P (kbar)[3]	1.6–2.3 (avg. 2.0)		2.0–2.6 (avg. 2.3)	2.6–4.0 (avg. 3.4)	1.0–2.0 (avg. 1.5)	2.0–3.2 (avg. 2.8)
T (°C)[4]	690–720	730–790	740–780	780–800	710–730	710–720
P (kbar)[5]	2.0–3.7 (avg. 2.7)	2.1–3.3 (avg. 2.9)	1.5–3.0 (avg. 2.6)	2.9–4.5 (avg. 4.1)	1.2–2.6 (avg. 2.1)	2.5–4.5 (avg. 3.7)
$\log \eta$ (Pa s)[6]	4.9–5.6		4.4–4.9	3.4–4.4	4.8–4.9	4.5–5.1
$\log f_{O_2}$ (ΔFMQ)[7]			2.2		2.2	1.5

[1] I = I type (arc related); A = A type (within plate)
[2] Estimated by using the water-by-difference method
[3] Minimum entrapment pressure based on the melt H_2O content and solubility data in the haplogranite system (Johannes and Holtz, 1996)
[4] Zircon saturation temperature according to Watson and Harrison (1983), using the original Zr concentrations measured in the melt inclusions
[5] Titanium-in-quartz (TitaniQ) pressure calculated according to the calibration of Huang and Audétat (2012)
[6] Magma viscosity calculated based on the model of Giordano et al. (2004)
[7] Oxygen fugacity based on molybdenite solubility models of Audétat et al. (2011) and Sun et al. (2014); ΔFMQ = relative to the fayalite-magnetite-quartz buffer
[8] Data from Mercer et al. (2015) and Zhang and Audétat (2017)
[9] Data from Zhang and Audétat (2017)
[10] Data from Audétat (2015)
[11] Data from Lowenstern (1994), Audétat et al. (2011), and Zhang and Audétat (2017)

In summary, at Yangjiazhangzi and Wanbaoyuan, the syn-mineralization intrusions tend to have crystallized at slightly lower temperatures than the premineralization intrusions (720°–695°C vs. 790°–730°C at Yangjiazhangzi, 720°–690°C vs. 770°–690°C at Wanbaoyuan), whereas the calculated pressure ranges are similar. At Hashitu, no systematic difference in the crystallization conditions of syn- vs. premineralization intrusions was observed.

Discussion

Apparent Mo-poor character of the mineralizing magmas

Metals in porphyry(-skarn) Mo deposits are derived from magmas from which metal-bearing fluids exsolved (Hedenquist and Lowenstern, 1994). Hence, a key consideration when evaluating the processes responsible for generation of porphyry Mo deposits is the Mo content of the mineralizing magmas. As summarized in Table 4, the mineralizing melts of the six deposits investigated in this study contained between 1 and 7 ppm Mo. The corresponding average of ~3 ppm Mo is distinctly lower than that reported for Climax-type deposits and barren intrusions (Fig. 8). It may be that the mineralizing melts at Hashitu were molybdenite saturated before growth of the melt inclusions; hence, the Mo content of the bulk magma may have been significantly higher. However, the molybdenite inclusions are too sparse to account for the loss of Mo. An alternative possibility for the low Mo content of the mineralizing magmas is that Mo had exsolved into the fluid phase before the magma was fully crystallized. As shown in Figure 8, Mo concentrations measured in melt inclusions

from the synmineralization samples of individual deposits correlate positively with Rb and Cs concentrations, suggesting the interpretation that the melts investigated in the present study are Mo poor is valid.

On the (Y + Nb) vs. Rb tectonic discrimination diagram of Pearce et al. (1984) and Pearce (1996), most of the mineralizing melts in this study plot within the syncollisional (S-type) granite field, whereas their corresponding whole-rock samples plot both in the volcanic arc (I-type) granite and syncollisional (S-type) granite fields (Fig. 7). This discrepancy may stem from the fact that this discrimination diagram was developed for granitic whole rocks, whereas residual liquids such as aplites, pegmatites, and many melt inclusions are distinctly more evolved and thus contain more Rb (Audétat, 2015). The I- and S-type natures of the mineralizing melts contrast with the melt inclusion compositions from Climax-type Mo deposits, which plot in the field of within-plate (A-type) granite (Audétat and Li, 2017; Fig. 7). Irrespective of whether they are I, S, or A type, these mineralizing magmas share a similar Mo-poor character (1–25 ppm; Mercer et al., 2015; Zhang and Audétat, 2017; Table 4). Therefore, we suggest that mineralizing magmas for porphyry(-skarn) Mo deposits are all Mo poor, regardless of the tectonic settings in which they formed. Magmatic Mo enrichment is therefore not necessary for forming porphyry Mo deposits.

Factors affecting Mo mineralization potential

Many stages in the formation of porphyry Mo deposits may have an impact on the mineralization potential, including the generation of melts in the source region, the buildup of the upper crustal magma chamber, the timing of fluid saturation, the efficiency of metal extraction by the exsolving fluids, and the efficiency of fluid focusing (e.g., Lerchbaumer and Audétat, 2013; Audétat and Li, 2017). Available isotope data show that Nd and Hf isotope compositions of mineralizing magmas investigated in this study are highly variable. For example, zircon Hf isotope compositions of the synmineralization rhyolite porphyry at Songbei ($\varepsilon_{Hf}(t)$ = –10.0 to –6.9) suggest an ancient lower-crustal source (Chu et al., 2017), while Nd and Hf isotopes of the ore-related monzogranite porphyries of Aolunhua ($\varepsilon_{Nd}(t)$ = 0.5–1.4; $\varepsilon_{Hf}(t)$ = 3.5–9.8) indicate a hybrid source between newly underplated basaltic crust and previously metasomatized lithospheric mantle (Ma et al., 2013). Neodymium isotope composition of the ore-related syenogranite intrusion at Hashitu ($\varepsilon_{Nd}(t)$ = 1.1–2.1) suggests a juvenile basaltic crust magma source (Ding et al., 2016). Independent of the exact nature of the source regions, these magmas were all able to produce major ($\geq$0.1 Mt Mo) porphyry(-skarn) Mo deposits. This implies that the magma source region for the formation of porphyry Mo deposits is not as important as the requirement for substantial volumes of hydrous felsic magma to be produced.

No systematic difference in the Mo content of the silicate melts in pre- vs. synmineralization intrusions is evident in any of the deposits studied (Fig. 8). This suggests that the Mo content of the silicate melt does not play a critical role for the formation of porphyry Mo deposits. It is possible that Mo was more efficiently extracted by aqueous fluids exsolved from the mineralizing intrusions than from the barren intrusions. Lerchbaumer and Audétat (2013), Audétat and Li (2017),

and Zhang and Audétat (2018) showed that the available data do not give any evidence for higher fluid-melt partition coefficients or higher Mo contents in the fluids of mineralizing intrusions. Thus, the efficiency of metal extraction by the exsolving fluids is unlikely to have been a significant factor in controlling mineralization.

The low Mo content of the mineralizing magmas implies that large magma volumes were required to provide all of the Mo present in the deposits (0.13–1.7 Mt Mo; Table 4). Assuming an extraction efficiency of 100%, a minimum of 24 km^3 of magma was required to produce mineralization at Yangjiazhangzi, $\geq$21 km^3 for Songbei, $\geq$20 km^3 at Lanjiagou, $\geq$315 km^3 at Aolunhua, $\geq$12 km^3 at Hashitu, and $\geq$22 km^3 at Wanbaoyuan. It is possible that the premineralization intrusions of each of these deposits failed to produce mineralization simply because they were too small. Previous estimates of minimum magma volumes for barren vs. mineralized intrusions did not reveal any systematic differences (Lerchbaumer and Audétat, 2013; Audétat and Li, 2017). Our results are consistent with their observations, because the premineralization pluton in the Songbei-Yangjiazhangzi-Lanjiagou district ($\geq$200 km^3; Fig. 2a) is much larger than that of the synmineralization intrusions (~4 km^3 at Lanjiagou). Two points should be noted here: (1) the rock volume of the synmineralization intrusion was defined by its exposed area in the field and thickness constrained by geologic cross section (Fig. 2c, d), and (2) for the premineralization pluton, exposed over an area of $\geq$10 $\times$ 20 km (Fig. 2a), a minimum thickness of 1 km was assumed.

The evidence presented above suggests that the potential for producing porphyry Mo mineralization is determined after the arrival of hydrous, Mo-poor magmas in the upper crust and does not relate to the Mo content of the fluid or to the magma volume. Other factors are likely to be the amount of fluid that exsolves from the intrusions (Lowenstern, 1995), the timing of fluid saturation (Bodnar et al., 2014), or how efficiently these fluids were focused (Shinohara et al., 1995; Audétat and Li, 2017). The amount of fluid exsolved depends primarily on the intrusion size and its original water content. Field relationships at Lanjiagou, Hashitu, and Wanbaoyuan suggest that the barren, precursor plutons were initially fluid undersaturated, whereas the ore-forming stocks were fluid saturated. Evidence includes the breccia bodies that formed at the rim of the synmineralization intrusion at Lanjiagou (Fig. 2c) and Mo-mineralized veins at Hashitu and Wanbaoyuan that emanate from the ore-forming stocks, but not from the precursor intrusion (Fig. 5c, d). Some of the barren plutons did not exsolve enough fluid to produce a deposit, but most of the granite compositions sensu stricto plot near the fluid-saturated eutectic in the quartz-albite-orthoclase diagram (Tuttle and Bowen, 1958), indicating that the barren intrusions should have been fluid saturated or at least close to saturation and thus could have exsolved significant volumes of fluid.

The estimated pressures at which the ore-forming magmas were emplaced were mostly within 2 to 1 kbar, corresponding to emplacement depths of 8 to 4 km at an average upper crustal density of 0.27 g/cm^3, similar to those reported from Climax-type deposits (6–2 km; White et al., 1981; Lerchbaumer and Audétat, 2013; Audétat and Li, 2017) and from porphyry Cu($\pm$Mo, Au) deposits (6–1 km; Seedorff et al., 2005). This highlights the fundamental role of magma emplacement

depth (impact on fluid saturation; Burnham, 1985) as a vital aspect of porphyry ore formation. There is no difference in emplacement depths calculated for the syn- and premineralization intrusions (Table 4), so not all of the intrusions that crystallized at this depth range induced Mo mineralization.

Another potential factor is magma viscosity, which determines how efficiently the evolved, residual melts can separate from a cooling crystal mush, and what will happen once significant volumes of such melts are amassed under the roof of the magma chamber (Lange, 1994; Baker and Vaillancourt, 1995; Giordano et al., 2004). Melt viscosities obtained from the deposits investigated in the present study (4.3–5.1 Pa s at Hashitu, 4.9–5.6 Pa s at Yangjiazhangzi, and 5.8–6.1 Pa s at Wanbaoyuan; Table 4) are higher than those calculated for Climax-type deposits (Audétat, 2015; Zhang and Audétat, 2017). However, in all cases the calculated melt viscosities plot at the lower end of the range of viscosities displayed by ordinary rhyolites (Fig. 9). Hence, porphyry-Mo–forming melts generally have relatively low viscosities, but there are exceptions, such as Wanbaoyuan. The barren Huangshan pluton studied by Zhang and Audétat (2018) showed similar low magma viscosities. The fluorine content of ore-forming magmas can reduce the viscosity of magmas significantly (Dingwell et al., 1985), and the high fluorine activity in Climax-type deposits indicates that fluorine may be important (e.g., Audétat, 2015). However, the mineralizing melts in this study contain ≤0.4 wt % F (Table 4), implying that fertile magmas in porphyry Mo systems do not necessarily have to be F rich.

It is concluded that the efficiency of fluid focusing has the biggest impact on mineralization potential. The efficiency of fluid focusing is controlled by the development of a cupola above the batholithic magma chamber, which acts as a conduit along which fluids can be focused (Burnham, 1979; Lowenstern, 1994; Shinohara et al., 1995). The premineralization intrusions investigated in this study are distinguished by tending to occur as batholiths (exposed area up to 200 km^2; Wu et al., 2006; Hu et al., 2007; Zhai et al., 2018), which may have inhibited the focusing of fluid flow. In contrast, the synmineralization intrusions were emplaced into the premineralization intrusions or wall rocks as vertically attenuated stocks, pipes, or dike swarms (Figs. 2, 5, App. Figs. S1, S2). It remains unclear as to what fundamentally controls the formation of cupolas, although deep faults linked with external triggers such as volcanic edifice collapse or megaearthquakes might be critical factors (Piquer et al., 2015; Richards, 2018).

Controls on Mo endowment

The deposits investigated in this study vary in size from 0.12 to 1.70 Mt. Despite their different metal endowments, their mineralizing melts have similar compositions and crystallization conditions. They have low Mo (1–7 ppm) and F (≤0.4 wt %) and elevated water contents (4.0–7.0 wt %) with crystallization temperatures of 770° to 690°C and emplacement depth between 8 and 4 km (Table 4). Similar characteristics have been documented for mineralizing melts from Climax-type deposits, although these melts are more evolved (3–10× more than average granite) and contain higher F (0.2–3.9 wt %; Audétat and Li, 2017) than the melts investigated in the present study. However, in all cases, there is no direct relationship between the compositions and crystallization conditions of mineralizing melts and Mo tonnages (Table
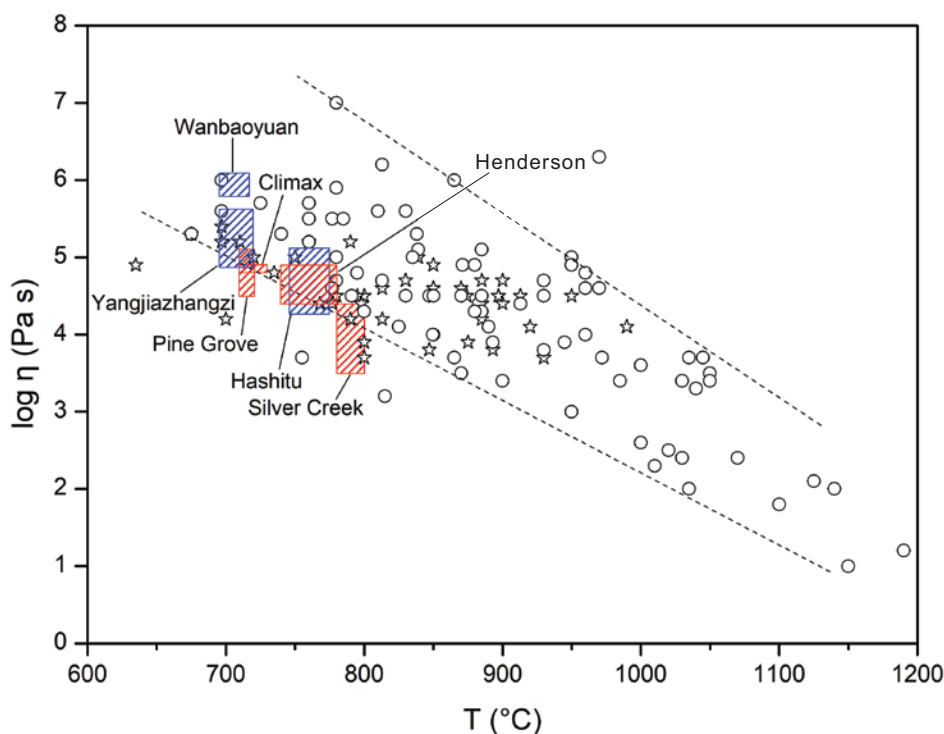

Fig. 9. Estimated viscosities of melt inclusions investigated in the present study (blue boxes), compared to estimates for melts associated with Climax-type porphyry deposits (red boxes, Zhang and Audétat, 2017). Preeruption magma viscosities of unmineralized mafic to felsic magmas are indicated by stars (Scaillet et al., 1998) and circles (Takeuchi, 2011).

4). Fluid inclusion LA-ICP-MS analysis results from Audétat (2015) and Audétat and Li (2017) did not reveal any significant variations in Mo contents of the fluids exsolved from the different mineralizing intrusions. Thus, we suggest that the difference in metal endowment lies in the fluid flux through the cupola, which, in turn, is controlled by the size of cupola and the duration of fluid release. The size of the mineralized intrusions investigated in this study cannot be constrained in the present study. Nevertheless, it could be that the volume of fluid release was the major control on metal endowment. The arguments are as follows: (1) the size of the individual synmineralization intrusion in porphyry Mo deposits is typically small (less than 500-m diameter; Lowenstern, 1994; Brown and Kahlert, 1995; Seedorff and Einaudi, 2004; Gaynor et al., 2019), and (2) evidence for multiple intrusive and vein-forming events is observed in many large porphyry Mo deposits (e.g., Urad-Henderson and Endako; Carten et al., 1988; Selby and Creaser, 2001; Seedorff and Einaudi, 2004).

Conclusions

Silicate melts in the synmineralization porphyry intrusions in northeastern China are one to four times more evolved than average granite. The silicate melts have Mo (1–7 ppm) and F ($\leq$0.4 wt %) depletion but were enriched in H_2O (4.0–7.0 wt %). Thermobarometric results suggest that the magma crystallized at 770° to 690°C and 3.7 to 1.0 kbar, which is within the typical range displayed by porphyry Mo and porphyry Cu deposits (e.g., Seedorff et al., 2005; Audétat and Li, 2017). The viscosity of the silicate melts (4.3–6.1 Pa s) is at the lower end of the range reported for other rhyolites at these temperatures.

Within individual deposits, no systematic differences in the degree of magma fractionation, crystallization conditions, Mo content of the silicate melt, and magma volume were noted between pre- and synmineralization intrusions. The only difference seems to be that the premineralization intrusions tend to occur as batholiths. Hence, the mineralization potential is most strongly controlled by fluid focus into and through a smaller rock volume. A prerequisite for this process is the formation of a cupola at the apex of a batholith, which is probably promoted by activated subvertical faults above the magma chamber (e.g., Piquer et al., 2015).

The results of this study indicate that magmatic Mo and F enrichment is not an essential prerequisite for porphyry Mo development. Molybdenum tonnages of porphyry Mo deposits have no direct relationship with the composition and crystallization condition history of mineralizing intrusions. The key factor is the volume of fluid released from the underlying magma chamber together with its focusing into a cupola (e.g., Carten et al., 1988; Seedorff and Einaudi, 2004).

Acknowledgments

REFERENCES

Alberico, A., Ferrando, S., Ivaldi, G., and Ferraris, G., 2003, X-ray single-crystal structure refinement of an OH-rich topaz from Sulu UHP terrane (eastern China)—structural foundation of the correlation between cell parameters and fluorine content: European Journal of Mineralogy, v. 15, p. 875–881.

Aseri, A.A., Linnen, R.L., Che, X.D., Thibault, Y., and Holtz, F., 2015, Effects of fluorine on the solubilities of Nb, Ta, Zr and Hf minerals in highly fluxed water-saturated haplogranitic melts: Ore Geology Reviews, v. 64, p. 736–746.

Audétat, A., 2010, Source and evolution of molybdenum in the porphyry Mo(-Nb) deposit at Cave Peak, Texas: Journal of Petrology, v. 51, p. 1739–1760.

——2013, Origin of Ti-rich rims in quartz phenocrysts from the Upper Bandelier Tuff and the Tunnel Spring Tuff, southwestern USA: Chemical Geology, v. 360–361, p. 99–104.

——2015, Compositional evolution and formation conditions of magmas and fluids related to porphyry Mo mineralization at Climax, Colorado: Journal of Petrology, v. 56, p. 1519–1546.

Audétat, A., and Li, W., 2017, The genesis of Climax-type porphyry Mo deposits: Insights from fluid inclusions and melt inclusions: Ore Geology Reviews, v. 88, p. 436–460.

Audétat, A., and Lowenstern, J.B., 2014, Melt inclusions, in Holland, H.D., and Turekian, K.K., eds., Treatise on geochemistry (second edition): Oxford, Elsevier, p. 143–173.

Audétat, A., and Pettke, T., 2003, The magmatic-hydrothermal evolution of two barren granites: A melt and fluid inclusion study of the Rito del Medio and Canada Pinabete plutons in northern New Mexico (USA): Geochimica et Cosmochimica Acta, v. 67, p. 97–121.

Audétat, A., Pettke, T., Heinrich, C.A., and Bodnar, R.J., 2008, The composition of magmatic-hydrothermal fluids in barren and mineralized intrusions: Economic Geology, v. 103, p. 877–908.

Audétat, A., Dolejs, D., and Lowenstern, J.B., 2011, Molybdenite saturation in silicic magmas: Occurrence and petrological implications: Journal of Petrology, v. 52, p. 891–904.

Audétat, A., Garbe-Schönberg, D., Kronz, A., Pettke, T., Rusk, B., Donovan, J.J., and Lowers, H.A., 2015, Characterisation of a natural quartz crystal as a reference material for microanalytical determination of Ti, Al, Li, Fe, Mn, Ga and Ge: Geostandards and Geoanalytical Research, v. 39, p. 171–184.

Baker, D.R., and Vaillancourt, J., 1995, The low viscosities of F+H_2O-bearing granitic melts and implications for melt extraction and transport: Earth and Planetary Science Letters, v. 132, p. 199–211.

Bali, E., Keppler, H., and Audétat, A., 2012, The mobility of W and Mo in subduction zone fluids and the Mo-W-Th-U systematics of island arc magmas: Earth and Planetary Science Letters, v. 351–352, p. 195–207.

Bodnar, R.J., Lecumberri-Sanchez, P., Moncada, D., and Steele-MacInnis, M., 2014, Fluid inclusions in hydrothermal ore deposits, in Holland, H.D., and Turekian, K.K., eds., Treatise on geochemistry (second edition): Oxford, Elsevier, p. 119–142.

Brown, P., and Kahlert, B., 1995, Geology and mineralization of the Red Mountain porphyry molybdenum deposit, south-central Yukon, in Schroeter, T.G., ed., Porphyry deposits of the northwestern Cordillera of North America, 46: Montreal, Canadian Institute of Mining, Metallurgy and Petroleum, p. 747–756.

Burnham, C.W., 1979, Magma and hydrothermal fluids, in Barnes, H.L., ed., Geochemistry of hydrothermal ore deposits: New York, Wiley, p. 71–136.

——1985, Energy release in subvolcanic environments: Implications for breccia formation: Economic Geology, v. 80, p. 1515–1522.

Carten, R.B., Geraghty, E.P., Walker, B.M., and Shannon, J.R., 1988, Cyclic development of igneous features and their relationship to high-temperature hydrothermal features in the Henderson porphyry molybdenum deposit, Colorado: Economic Geology, v. 83, p. 266–296.

Carten, R.B., White, W.H., and Stein, H.J., 1993, High-grade granite-related molybdenum systems: Classification and origin: Geological Association of Canada, Special Paper 40, p. 521–554.

Chen, B., Zhai, M.G., and Tian, W., 2007, Origin of the Mesozoic magmatism in the North China craton: Constraints from petrological and geochemical data: Geological Society, London, Special Publications, v. 280, p. 131–151.

Chen, Y.J., Zhang, C., Li, N., Yang, Y.F., and Deng, K., 2012, Geology of the Mo deposits in northeast China: Journal of Jilin University (Earth Science Edition), v. 42, p. 1223–1368 (in Chinese with English abstract).

Chen, Y.J., Wang, P., Li, N., Yang, Y.F., and Pirajno, F., 2017, The collision-type porphyry Mo deposits in Dabie Shan, China: Ore Geology Reviews, v. 81, p. 405–430.

Chu, S.X., Zeng, Q.D., and Liu, J.M., 2017, Re-Os and U-Pb geochronology of the Songbei porphyry-skarn Mo deposit, North China craton: Implications for the Early Jurassic tectonic setting in eastern China: Journal of Geochemical Exploration, v. 181, p. 256–269.

Dai, J.Z., Mao, J.W., Zhao, C.S., Li, F.R., Wang, R.T., Xie, G.Q., and Yang, F.Q., 2008, Zircon SHRIMP U-Pb age and petrogeochemical features of Lianjiagou granite in western Liaoning Province: Acta Geologica Sinica, v. 82, p. 1555–1564 (in Chinese with English abstract).

Davis, G.A., Zheng, Y., Wang, C., Darby, B.J., Zhang, C., and Gehrels, G.E., 2001, Mesozoic tectonic evolution of the Yanshan fold and thrust belt, with emphasis on Hebei and Liaoning provinces, northern China, in Hendrix, M.S., and Davis, G.A., eds., Paleozoic and Mesozoic tectonic evolution of central and eastern Asia: From continental assembly to intracontinental deformation: Geological Society of America Memoir, p. 171–197.

Devine, J.D., Gardner, J.E., Brack, H.P., Laynet, G.D., and Rutherford, M.J., 1995, Comparison of microanalytical methods for estimating H₂O contents of silicic volcanic glasses: American Mineralogist, v. 80, p. 319–328.

Ding, C.W., Dai, P., Bagas, L., Nie, F.J., Jiang, S.H., Wei, J.H., Ding, C.Z., Zuo, P.F., and Zhang, K., 2016, Geochemistry and Sr-Nd-Pb isotopes of the granites from the Hashitu Mo deposit of Inner Mongolia, China: Constraints on their origin and tectonic setting: Acta Geologica Sinica (English edition), v. 90, p. 106–120.

Dingwell, D.B., Scarfe, M.C., and Cronin, D.J., 1985, The effect of fluorine on viscosities in the system Na_2O-Al_2O_3-SiO_2: Implications for phonolites, trachytes and rhyolites: American Mineralogist, v. 70, p. 80–87.

Donovan, J., and Vicenzi, E., 2008, Water by EPMA—new developments: Microscopy and Microanalysis, v. 14, p. 1266–1274.

Frezzotti, M.L., 2001, Silicate-melt inclusions in magmatic rocks: Applications to petrology: Lithos, v. 55, p. 273–299.

Gao, S., Rudnick, R.L., Yuan, H.L., Liu, X.M., Liu, Y.S., Xu, W.L., Ling, W.L., Ayers, J., Wang, X.C., and Wang, Q.H., 2004, Recycling lower continental crust in the North China craton: Nature, v. 432, p. 892–897.

Gaynor, S.P., Rosera, J.M., and Coleman, D.S., 2019, Intrusive history of the Oligocene Questa porphyry molybdenum deposit, New Mexico: Geosphere, v. 15, p. 548–575.

Giordano, D., Romano, C., Dingwell, D.B., Poe, B., and Behrens, H., 2004, The combined effects of water and fluorine on the viscosity of silicic magmas: Geochimica et Cosmochimica Acta, v. 68, p. 5159–5168.

Guillong, M., and Heinrich, C.A., 2007, Sensitivity enhancement in laser ablation ICP-MS using small amounts of hydrogen in the carrier gas: Journal of Analytical Atomic Spectrometry, v. 22, p. 1488–1494.

Guo, F., Fan, W.M., Li, X.Y., and Li, C.W., 2007, Geochemistry of Mesozoic mafic volcanic rocks from the Yanshan belt in the northern margin of the North China block: Relations with post-collisional lithospheric extension: Geological Society, London, Special Publications, v. 280, p. 101–129.

Halter, W.E., Pettke, T., Heinrich, C.A., and Rothen-Rutishauser, B., 2002, Major to trace element analysis of melt inclusions by laser-ablation ICP-MS: Methods of quantification: Chemical Geology, v. 183, p. 63–86.

Han, C.M., Xiao, W.J., Zhao, G.C., Sun, M., Qu, W.J., and Du, A.D., 2009, A Re-Os study of molybdenites from the Lanjiagou Mo deposit of North China craton and its geological significance: Gondwana Research, v. 16, p. 264–271.

Hedenquist, J.W., and Lowenstern, J.B., 1994, The role of magmas in the formation of hydrothermal ore deposits: Nature, v. 370, p. 519–527.

Hu, T.J., Zhang, Y.N., and Liu, Z.Y., 2007, General exploration report of the Wanbaoyuan molybdenum deposit in Dandong City, Liaoning Province: Shengyang, Liaoning Non-ferrous Geological Exploration and Research Institute Co., Ltd., 109 p.

Huang, D.H., Dong, Q.Y., and Gan, Z.X., 1989, China molybdenum deposits, in Song, S.H., ed., China deposits: Beijing, Geology Publishing House, p. 493–536 (in Chinese with English abstract).

Huang, D.H., Wu, C.Y., Du, A.D., and He, H.L., 1994, Re-Os ages molybdenum deposits in east Qinling and their significance: Mineral Deposits, v. 13, p. 221–230 (in Chinese with English abstract).

Huang, R., and Audétat, A., 2012, The titanium-in-quartz (TitaniQ) thermobarometer: A critical examination and re-calibration: Geochimica et Cosmochimica Acta, v. 84, p. 75–89.

Johannes, W., and Holtz, F., 1996, Petrogenesis and experimental petrology of granitic rocks: Berlin, Springer, v. 22, p. 1–329.

Keppler, H., 1993, Influence of fluorine on the enrichment of high field strength trace elements in granitic rocks: Contributions to Mineralogy and Petrology, v. 114, p. 479–488.

Kularatne, K., and Audétat, A., 2014, Rutile solubility in hydrous rhyolite melts at 750–900°C and 2 kbar, with application to titanium-in-quartz (TitaniQ) thermobarometry: Geochimica et Cosmochimica Acta, v. 125, p. 196–209.

Lange, R.A., 1994, The effects of H_2O, CO_2 and F on the density and viscosity of silicate melts: Reviews in Mineralogy and Geochemistry, v. 30, p. 331–369.

Lerchbaumer, L., and Audétat, A., 2013, The metal content of silicate melts and aqueous fluids in subeconomically Mo mineralized granites: Implications for porphyry Mo genesis: Economic Geology, v. 108, p. 987–1013.

Li, J.W., Bi, S.J., Selby, D., Chen, L., Vasconcelos, P., Thiede, D., Zhou, M.F., Zhao, X.F., Li, Z.K., and Qiu, H.N., 2012, Giant Mesozoic gold provinces related to the destruction of the North China craton: Earth and Planetary Science Letters, v. 349–350, p. 26–37.

Lowenstern, J.B., 1994, Dissolved volatile concentrations in an ore-forming magma: Geology, v. 22, p. 893–896.

——1995, Application of silicate-melt inclusions to the study of magmatic volatiles, in Thompson, J.F.H., ed., Magmas, fluids and ore deposition: Victoria, Mineralogical Association of Canada, p. 71–99.

Ludington, S., and Plumlee, G.S., 2009, Climax-type porphyry molybdenum deposits, U.S.: United States Geological Survey Open-File Report, 16 p.

Ma, X.H., Chen, B., Lai, Y., and Lu, Y.H., 2009, Petrogenesis and mineralization chronology study on the Aolunhua porphyry Mo deposit, Inner Mongolia, and its geological implications: Acta Petrologica Sinica, v. 25, p. 2939–2950.

Ma, X.H., Chen, B., and Yang, M.C., 2013, Magma mixing origin for the Aolunhua porphyry related to Mo-Cu mineralization, eastern Central Asian orogenic belt: Gondwana Research, v. 24, p. 1152–1171.

Meng, Q.R., 2003, What drove late Mesozoic extension of the northern China-Mongolia tract?: Tectonophysics, v. 369, p. 155–174.

Mercer, C.N., Hofstra, A.H., Todorov, T.I., Roberge, J., Burgisser, A., Adams, D.T., and Cosca, M., 2015, Pre-eruptive conditions of the Hideaway Park topaz rhyolite: Insights into metal source and evolution of magma parental to the Henderson porphyry molybdenum deposit, Colorado: Journal of Petrology, v. 56, p. 645–679.

Ouyang, H.G., Mao, J.W., Santosh, M., Zhou, J., Zhou, Z.H., Wu, Y., and Hou, L., 2013, Geodynamic setting of Mesozoic magmatism in NE China and surrounding regions: Perspectives from spatio-temporal distribution patterns of ore deposits: Journal of Asian Earth Sciences, v. 78, p. 222–236.

Pearce, J.A., 1996, Sources and settings of granitic rock: Episodes, v. 19, p. 120–125.

Pearce, J.A., Harris, N.B., and Tindle, A.G., 1984, Trace element discrimination diagrams for the tectonic interpretation of granitic rocks: Journal of Petrology, v. 25, p. 956–983.

Piquer, J., Skarmeta, J., and Cooke, D.R., 2015, Structural evolution of the Rio Blanco-Los Bronces district, Andes of central Chile: Controls on stratigraphy, magmatism, and mineralization: Economic Geology, v. 110, p. 1995–2023.

Richards, J.P., 2018, A shake-up in the porphyry world?: Economic Geology, v. 113, p. 1225–1233.

Rudnick, R.L., and Gao, S., 2003, The composition of the continental crust, in Holland, H.D., and Turekian, K.K., eds., The crust, treatise on geochemistry: Oxford, Elsevier-Pergamon, p. 1–64.

Scaillet, B., Holtz, F., and Pichavant, M., 1998, Phase equilibrium constraints on the viscosity of silicic magmas: 1. Volcanic-plutonic comparison: Journal of Geophysical Research: Solid Earth, v. 103, p. 27,257–27,266.

Seedorff, E., and Einaudi, M.T., 2004, Henderson porphyry molybdenum system, Colorado: I. Sequence and abundance of hydrothermal mineral assemblages, flow paths of evolving fluids, and evolutionary style: Economic Geology, v. 99, p. 3–37.

Seedorff, E., Dilles, J.H., Proffett, Jr., J.M., Einaudi, M.R., Zurcher, L., Stavast, W.J.A., Johnson, D.A., and Barton, M.D., 2005, Porphyry copper deposits: Characteristics and origin of hypogene features: Economic Geology 100th Anniversary Volume, p. 251–298.

Selby, D., and Creaser, R.A., 2001, Re-Os geochronology and systematics in molybdenite from the Endako porphyry molybdenum deposit, British Columbia, Canada: Economic Geology, v. 96, p. 197–204.

Shinohara, H., Kazahaya, K., and Lowenstern, J.B., 1995, Volatile transport in a convecting magma column: Implications for porphyry Mo mineralization: Geology, v. 23, p. 1091–1094.

Song, J.C., Hu, T.J., Wang, E.D., and Li, J.C., 2010, Geological characteristic and ore-forming mechanism of Wanbaoyuan Mo deposit in Kuandian, Liaoning Province: Global Geology, v. 29, p. 45–51 (in Chinese with English abstract).

Sun, S.S., and McDonough, W.F., 1989, Chemical and isotopic systematics of oceanic basalts: Implications for mantle composition and processes: Geological Society of America, Special Publication 42, p. 313–345.

Sun, W., Audétat, A., and Dolejs, D., 2014, Solubility of molybdenite in hydrous granitic melts at 800°C, 100–200 MPa: Geochimica et Cosmochimica Acta, v. 131, p. 393–401.

Takeuchi, S., 2011, Preeruptive magma viscosity: An important measure of magma eruptibility: Journal of Geophysical Research: Solid Earth, doi:10.1029/2011JB008243.

Taylor, R.D., Hammarstrom, J.M., Piatak, N.M., and Seal, II, R.R., 2012, Arc-related porphyry molybdenum deposit model: U.S. Geological Survey, U.S. Geological Survey, Scientific Investigations Report 2010-5070-D, p. 64.

Taylor, S.R., 1964, Abundance of chemical elements in the continental crust: A new table: Geochimica et Cosmochimica Acta, v. 28, p. 1273–1285.

Tuttle, O.F., and Bowen, N.L., 1958, Origin of granite in the light of experimental studies in the system, $NaAlSi_3O_8$-$KAlSi_3O_8$-SiO_2-H_2O: Geological Society of America, v. 74, p. 1–153.

U.S. Geological Survey, 2017, Mineral commodity summaries 2017: Reston, U.S. Geological Survey, 202 p.

Wang, F., Zhou, X.H., Zhang, L.C., Ying, J.F., Zhang, Y.T., Wu, F.Y., and Zhu, R.X., 2006, Late Mesozoic volcanism in the Great Xing'an Range (NE China): Timing and implications for the dynamic setting of NE Asia: Earth and Planetary Science Letters, v. 251, p. 179–198.

Watson, B.E., and Harrison, M.T., 1983, Zircon saturation revisited: Temperature and composition effects in a variety of crystal magma types: Earth and Planetary Science Letters, v. 64, p. 295–304.

Webster, J.D., 2006, Melt inclusions in plutonic rocks: Montreal, Mineralogical Association of Canada, 211 p.

Whalen, J.B., Anderson, R.G., Struik, L.C., and Villeneuve, M.E., 2001, Geochemistry and Nd isotopes of the François Lake plutonic suite, Endako batholith: Host and progenitor to the Endako molybdenum camp, central British Columbia: Canadian Journal of Earth Sciences, v. 38, p. 603–618.

White, W.H., Bookstrom, A.A., Kamilli, R.J., Ganster, M.W., Smith, R.P., Ranta, D.E., and Steininger, R.C., 1981, Character and origin of Climax-type molybdenum deposits: Economic Geology 75th Anniversary Volume, p. 270–316.

Wu, F.Y., Lin, J.Q., Wilde, S.A., Zhang, X.O., and Yang, J.H., 2005, Nature and significance of the Early Cretaceous giant igneous event in eastern China: Earth and Planetary Science Letters, v. 233, p. 103–119.

Wu, F.Y., Yang, J.H., Zhang, H.B., and Liu, X.M., 2006, Emplacement ages of the Mesozoic granites in southeastern part of the western Liaoning Province: Acta Petrological Sinica, v. 22, p. 315–325.

Wu, F.Y., Sun, D.Y., Ge, W.C., Zhang, Y.B., Grant, M.L., Wilde, S.A., and Jahn, B.M., 2011, Geochronology of the Phanerozoic granitoids in northeastern China: Journal of Asian Earth Sciences, v. 41, p. 1–30.

Wu, L.R., Zhang, X.Q., and Sun, S.H., 1990, On the magma generation, evolution and molybdenum mineralization of the Yangjiazhangzi Complex, Jinxi, Liaoning Province: Acta Petrologica Sinica, v. 3, p. 1–11 (in Chinese with English abstract).

Xiao, W., Windley, B.F., Hao, J., and Zhai, M., 2003, Accretion leading to collision and the Permian Solonker suture, Inner Mongolia, China: Termination of the central Asian orogenic belt: Tectonics, doi:10.1029/2002TC001484.

Xu, W.L., Gao, S., Wang, Q.H., Wang, D.Y., and Liu, Y.S., 2006, Mesozoic crustal thickening of the eastern North China craton: Evidence from eclogite xenoliths and petrologic implications: Geology, v. 34, p. 721–724.

Xu, W.L., Pei, F.P., Wang, F., Meng, E., Ji, W.Q., and Yang, D.B., 2013, Spatial-temporal relationships of Mesozoic volcanic rocks in NE China: Constraints on tectonic overprinting and transformations between multiple tectonic regimes: Journal of Asian Earth Sciences, v. 74, p. 167–193.

Yang, J.H., Wu, F.Y., Shao, J.A., Wilde, S.A., Xie, L.W., and Liu, X.M., 2006, Constraints on the timing of uplift of the Yanshan fold and thrust belt, north China: Earth and Planetary Science Letters, v. 246, p. 336–352.

Yang, Z.Z., Chen, S.L., and Dong, W.D., 1989, Regional geology of Liaoning Province: Beijing, Geological Publishing House, 321 p.

Zajacz, Z., Hanley, J.J., Heinrich, C.A., Halter, W.E., and Guillong, M., 2009, Diffusive reequilibration of quartz-hosted silicate melt and fluid inclusions: Are all metal concentrations unmodified?: Geochimica et Cosmochimica Acta, v. 73, p. 3013–3027.

Zeng, Q.D., Liu, J.M., Qin, K.Z., Fan, H.R., Chu, S.X., Wang, Y.B., and Zhou, L.L., 2013, Types, characteristics, and time-space distribution of molybdenum deposits in China: International Geology Review, v. 55, p. 1311–1358.

Zhai, D.G., Liu, J.J., Wang, J.P., Yang, Y.Q., Zhang, H.Y., Wang, X.L., Zhang, Q.B., Wang, G.W., and Liu, Z.J., 2014, Zircon U-Pb and molybdenite Re-Os geochronology, and whole-rock geochemistry of the Hashitu molybdenum deposit and host granitoids, Inner Mongolia, NE China: Journal of Asian Earth Sciences, v. 79, p. 144–160.

Zhai, D.G., Liu, J.J., Tombros, S., and Williams-Jones, A.E., 2018, The genesis of the Hashitu porphyry molybdenum deposit, Inner Mongolia, NE China: Constraints from mineralogical, fluid inclusion, and multiple isotope (H, O, S, Mo, Pb) studies: Mineralium Deposita, v. 53, p. 377–397.

Zhang, D.H., and Audétat, A., 2017, Chemistry, mineralogy and crystallization conditions of porphyry Mo-forming magmas at Urad-Henderson and Silver Creek, Colorado, USA: Journal of Petrology, v. 58, p. 277–296.

——2018, Magmatic-hydrothermal evolution of the barren Huangshan pluton, Anhui Province, China: A melt and fluid inclusion study: Economic Geology, v. 113, p. 803–824.

Zhang, S.H., Zhao, Y., Davis, G.A., Ye, H., and Wu, F., 2014, Temporal and spatial variations of Mesozoic magmatism and deformation in the North China craton: Implications for lithospheric thinning and decratonization: Earth-Science Reviews, v. 131, p. 49–87.

Zheng, Y.C., Feng, H., Wu, C.Z., Gu, L.X., Liu, S.H., and He, K., 2014, Influence of crude oil on the genesis of the Lanjiagou porphyry molybdenum deposit, western Liaoning Province, China: Ore Geology Reviews, v. 60, p. 1–13.

Hegen Ouyang is currently an associate professor at the Institute of Mineral Resources, Chinese Academy of Geological Sciences. He received a Ph.D. degree in economic geology from the China University of Geosciences (Beijing) in 2013 and a master's degree from the Institute of Oceanology Chinese Academy of Sciences in 2010. Hegen's research interests include factors affecting porphyry mineralization potential, as well as the temporal and spatial evolution of magmatic-hydrothermal ore systems.